

Nonlinear dynamics and chaotic motions in feedback controlled two and three-degree-of-freedom robots

A.S. Ravishankar and Ashitava Ghosal*

Abstract

The dynamics of a feedback controlled rigid robot is most commonly described by a set of nonlinear ordinary differential equations. In this paper, we analyse these equations, representing the feedback controlled motion of two and three-degree-of-freedom rigid robots with revolute(R) and prismatic(P) joints in the absence of compliance, friction and potential energy, for the possibility of chaotic motions. We first study the unforced or inertial motions of the robots and show that when the Gaussian or Riemannian curvature of the configuration space of a robot is negative, the robot equations can exhibit chaos. If the curvature is zero or positive, then the robot equations cannot exhibit chaos. We show that among the two-degree-of-freedom robots, the PP and the PR robot have zero Gaussian curvature while the RP and RR robot have negative Gaussian curvature. For the three-degree-of-freedom robots, we analyse the two well-known RRP and RRR configuration of the Stanford Arm and the PUMA manipulator respectively, and derive the conditions for negative curvature and possible chaotic motions.

The criteria of negative curvature cannot be used for the forced or the feedback controlled motions. For the forced motion, we resort to the well-known numerical techniques and compute chaos maps, Poincaré maps and bifurcation diagrams. Numerical results are presented for the two-degree-of-freedom RP and RR robots, and we show that these robot equations can exhibit chaos for low controller gains and for large underestimated models. From the bifurcation diagrams, the route to chaos appear to be through period doubling.

1 Introduction

The study of chaos in dynamical systems often involves the study of the mathematical equations in the form of nonlinear differential equations or maps which model the system. In mechanical systems, nonlinearities arise from a number of sources – Coriolis and centripetal

*The authors are with the Department of Mechanical Engineering, Indian Institute of Science, Bangalore-560 012, INDIA. (e-mail: asitava@mecheng.iisc.ernet.in)

accelerations or gravity associated with the motion of pendulum and other multi-body systems, nonlinear constitutive relations between stress and strain, nonlinear forces like magnetic, electric or coulombic friction, and geometric nonlinearities associated with large deformations in structural solids such as beams, plates and shells. Several mechanical systems with such non-linearities have been analysed for chaotic behavior(see for example (Guckenheimer and Holmes 1983; Moon 1987; Sekar and Narayanan 1992; Dowell and Pezeshki 1986; Tongue 1986; D’Humieres, Beasley, Huberman and Lichaber 1982; Hübinger, Doerner, Heng and Martienssen 1994*a*; Hübinger, Doerner, Heng and Martienssen 1994*b*; Hübinger, Doerner, Heng and Martienssen 1994*c*)). In this paper, we look at a different class of mechanical systems, namely that of feedback controlled rigid robots. A multi-link, feedback controlled, rigid robot is best modeled by a set non-linear ordinary differential equations with the non-linearity arising from the configuration dependent inertia and the non-linear control laws(Craig 1989). Unlike the large number of mechanical systems studied in chaos literature, there are no non-linearities resulting from motion under gravity or from non-linear mechanical elements such as springs, backlash and friction. In addition, the simplest set of equation, that of a planar two-degree-of-freedom robot, is 4 dimensional and non-autonomous and thereby more complicated than the typical 2 and 3 dimensional systems studied in literature. In this paper, we show that under certain conditions, involving the type, geometry and the control gains, a robot can exhibit chaotic motions and this suggests a re-look at some of the robustness results in robot control.

Although there exists a vast amount of literature on chaotic motions in mechanical systems such as Duffing’s oscillator and pendulum, the literature on chaos in robots is more limited. Vakakis and Burdick (Vakakis and Burdick 1990; Vakakis and Burdick 1991) have studied the dynamics of a simplified hopping robot where the non-linearity is in the form of a non-linear spring. M’closeky and Burdick(M’Closkey and Burdick 1993) have extended this model to a two-degree-of-freedom system, by including the forward running dynamics. The bifurcations diagrams which captures the variations in dynamical behavior with respect to the variations in the system and control parameters exhibit a period doubling cascade. Buhler and Koditschek(Bühler and Koditschek 1991) have studied a simplified planar juggling robot in the form of a nonlinear map. They observed that for certain lower order, local (linearised) stability properties determine the essential global(nonlinear) stability properties and that successive increments in the controller gain settings give rise to a cascade of period doubling bifurcations leading to chaos. Verghese et. al(Varghese, Fuchs and Mukundan 1991) have shown that the zero dynamics in a kinematically redundant robot controlled by a feedback linearisation technique can exhibit quasiperiodic and chaotic behavior. Streit et. al (Streit, Krousgrill and Bajaj 1986) have studied the nonlinear response in a flexible manipulator with a prismatic and revolute joints performing repetitive tasks. They have shown that the compliant coordinates can execute small but finite amplitude motions and in one particular case it has been shown that the amplitude of these periodic motion bifurcate to periodic solution which subsequently undergoes period doubling bifurcations leading to chaotic motions. Mahout et. al(Mahout, Lopez, Carcassés and Mira 1993) have shown that

a 2R manipulator with periodic forcing at the joints exhibits chaotic behavior for certain values of parameters. Shrinivas and Ghosal(Shrinivas and Ghosal 1996) have demonstrated that the nonlinear ordinary differential equations describing the motion of a feedback controlled rigid planar 2R robot undergoing repetitive motions can exhibit chaotic motion for a proportional plus derivative(PD) and a model based controller. Chaotic motions have been observed if the system is grossly under-damped and for low values of controller gains. Some experimental chaotic results were obtained by Mahout(Mahout 1994), on a 2R rigid manipulator with two electric actuators in the presence of friction.

The above mentioned works on chaos in robots, with the exception of Mahout(Mahout 1994), are especially numerical in nature. In this paper, apart from numerical results, we also propose an analytical approach to study chaos in unforced mechanical systems by making use of concepts from differential geometry. The paper is organised as follows: In section 2, we present in brief, the well known dynamic and feedback control equations of rigid robots. In section 3, we present an analytical criteria for chaos in unforced mechanical systems derived from the Gaussian and Riemannian curvature of the configuration space of a robot, and in section 4, we develop analytical expressions for several two and three-degree-of-freedom robots with prismatic(P) and revolute(R) joints. In section 5, we present a numerical study of the nonlinear equations describing an RP and RR manipulator undergoing repetitive motion in a horizontal plane under two well known robot control schemes, namely a simple PD control law and a model based control law. We present numerical results in the form of chaos maps giving values of gains for which the motion is chaotic, and the well known Poincaré map and bifurcation diagrams. Finally in section 6, we present our conclusions.

2 Dynamic modeling and control of rigid robots

The dynamics of rigid serial robot having n joints, in the absence of friction, can be written as

$$\mathbf{M}(\boldsymbol{\theta})\ddot{\boldsymbol{\theta}} + \mathbf{C}(\boldsymbol{\theta}, \dot{\boldsymbol{\theta}}) = \boldsymbol{\Gamma} \quad (1)$$

where, $\boldsymbol{\theta}(t)$ is the $n \times 1$ vector of joint angles, $\mathbf{M}(\boldsymbol{\theta})$ is the mass matrix, $\mathbf{C}(\boldsymbol{\theta}, \dot{\boldsymbol{\theta}})$ is the $n \times 1$ vector comprising of Coriolis and centrifugal torques and gravity terms, and $\boldsymbol{\Gamma}$ is the vector of joint torques/forces (Craig 1989).

The purpose of the robot arm controller is to ensure that the robot tracks a desired trajectory inspite of parameter uncertainties and external disturbances. A number of control schemes exists to achieve this purpose and they range from the simple independent joint control schemes to a more sophisticated adaptive control schemes(Craig 1988). We consider two well known control laws(Craig 1989), namely, (i) proportional plus derivative (PD) control and (ii) model based control.

For the PD controller, the torque at the joint i is calculated as

$$\Gamma_{p_i} = \ddot{\theta}_{d_i} + K_{v_i}(\dot{\theta}_{d_i}(t) - \dot{\theta}_i(t)) + K_{p_i}(\theta_{d_i}(t) - \theta_i(t)) \quad (2)$$

where, $\theta_{d_i}(t)$ is the desired trajectory to be tracked in joint space, $\theta_i(t)$ is the achieved (measured) trajectory, K_{p_i} and K_{v_i} are the positive proportional and derivative gains. It can be shown that, in the absence of gravity, the PD control law is asymptotically stable for a set-point or a regulator problem (where the desired velocity at the joints are zero) (Asada and Slotline 1986) in the sense of Lyapunov.

For the model based control, the joint torques are calculated as

$$\Gamma = \widehat{\mathbf{M}}(\boldsymbol{\theta})\Gamma_p + \widehat{\mathbf{C}}(\boldsymbol{\theta}, \dot{\boldsymbol{\theta}}) \quad (3)$$

where, $\Gamma_p = \ddot{\boldsymbol{\theta}}_d + \mathbf{K}_v(\dot{\boldsymbol{\theta}}_d - \dot{\boldsymbol{\theta}}) + \mathbf{K}_p(\boldsymbol{\theta}_d - \boldsymbol{\theta})$, $\widehat{\mathbf{M}}(\boldsymbol{\theta})$ is the estimated mass matrix, $\widehat{\mathbf{C}}(\boldsymbol{\theta}, \dot{\boldsymbol{\theta}})$ is the estimated Coriolis and centripetal torques vector, and \mathbf{K}_p , \mathbf{K}_v are positive definite constant diagonal gain matrices. Craig (Craig 1988) has given a robustness conjecture for the model based computed torque scheme which states that if $\widehat{\mathbf{M}}(\boldsymbol{\theta}) > 0$ and symmetric and $\mathbf{K}_v > \alpha * \mathbf{I}_n$ (where α is a positive number and \mathbf{I}_n is the $n \times n$ identity matrix), then the system is L_∞ stable. This result is justified by numerical simulation results, however, as far as we are aware there exists no proof of this conjecture in literature.

In this paper, we show that the nonlinear differential equations of a feedback controlled robot, under a PD or a model based control scheme, can exhibit *bounded chaotic* behavior and hence the robustness results are not strictly valid. In this paper, we assume that the robots perform a repetitive task, such as painting, in the absence of gravity and friction, and the desired joint space trajectories are of the form,

$$\theta_{d_i} = A_i \sin(\omega_i t), \quad i = 1, \dots, n \quad (4)$$

where A_i is the amplitude and ω_i is the frequency. For the above joint space trajectory, the end-effector of the robot repetitively traces a curve in Cartesian space.

Substitution of equation (4) in (3) results in a system of $2n$ first order ordinary differential equations which are coupled, nonlinear and non-autonomous. The equations are dissipative and the amount of dissipation is determined by the velocity gain \mathbf{K}_v . It is very difficult to derive any analytical results from such a general system of $2n$ first order nonlinear differential equations. As a first step we look at the unforced or the so-called inertial equations in the next section and derive analytical conditions for possible chaotic motions. We show that if the Gaussian curvature is negative in a 2D subspace, then the system of equations can exhibit chaos and if all the Riemannian symbols identically vanish then the equations cannot exhibit chaos. In section 5, we resort to numerical simulations to study the forced equations.

3 Analytical criteria for chaos for inertial motions

Before we introduce an analytical criteria for chaos for inertial motions, we introduce some required concepts from differential geometry (Stoker 1969) and classical dynamics (Arnold 1989).

In the absence of friction and a potential energy (in our case gravity), the Lagrangian of a n degree-of-freedom manipulator is only a function of the kinetic energy and is given by

$$L(\boldsymbol{\theta}, \dot{\boldsymbol{\theta}}) = (1/2) \dot{\boldsymbol{\theta}}^T [M(\boldsymbol{\theta})] \dot{\boldsymbol{\theta}} \quad (5)$$

It may be noted that $[M(\boldsymbol{\theta})]$ is a positive definite $n \times n$ matrix and its elements M_{ij} define a Riemannian metric in the configuration space (space of joint variables $\boldsymbol{\theta}$) of the manipulator. Once such a metric is defined in a space, we can compute the Riemannian curvature by constructing a covariant tensor of order 4, called the curvature tensor with components R_{ijkl} , as

$$R_{ijkl} = \sum_{h=1}^n M_{ih} R_{ikh}^h \quad (6)$$

where

$$\begin{aligned} R_{ijk}^l &= \frac{\partial \Gamma_{ik}^l}{\partial \theta_j} - \frac{\partial \Gamma_{ij}^l}{\partial \theta_k} + \sum_{h=1}^n [\Gamma_{ik}^h \Gamma_{hj}^l - \Gamma_{ij}^h \Gamma_{hk}^l] \\ \Gamma_{ij}^l &= \frac{1}{2} \sum_{k=1}^n M^{kl} \left(\frac{\partial M_{ik}}{\partial \theta_j} - \frac{\partial M_{ij}}{\partial \theta_k} + \frac{\partial M_{kj}}{\partial \theta_i} \right) \end{aligned} \quad (7)$$

In the above equations M^{kl} are the components of $[M(\boldsymbol{\theta})]^{-1}$ and the components Γ_{ij}^k are known as the Christoffel symbols of the second kind.

In the absence of potential energy, the equations of motion are given by the Hamilton's equations

$$\begin{aligned} \dot{\boldsymbol{\theta}} &= \frac{\partial H}{\partial \mathbf{p}} \\ \dot{\mathbf{p}} &= -\frac{\partial H}{\partial \boldsymbol{\theta}} + \Gamma \end{aligned} \quad (8)$$

where \mathbf{p} is the momentum and $H(\mathbf{p}, \boldsymbol{\theta})$ is the Hamiltonian¹.

Further one can define a canonical nonlinear transformation

$$\begin{aligned} \mathbf{P} &= \mathbf{P}(\mathbf{p}, \boldsymbol{\theta}) \\ \Theta &= \Theta(\mathbf{p}, \boldsymbol{\theta}) \end{aligned} \quad (9)$$

which ensures $\mathbf{p}^T d\boldsymbol{\theta} = \mathbf{P}^T d\Theta$. The function Θ which preserves the Riemannian metric is called an isometry, and it can be shown that the invariant which determines the Riemannian manifolds upto isometry is the Riemannian curvature, R_{ijkl} . When all the quantities R_{ijkl} identically vanish, one can show (Stoker 1969; Spong 1992) that the mass matrix $[M(\boldsymbol{\theta})]$ can

¹The momentum and Hamiltonian is related to the Lagrangian as $\mathbf{p} = \frac{\partial L}{\partial \dot{\boldsymbol{\theta}}}$ and $H(\mathbf{p}, \boldsymbol{\theta}) = \dot{\boldsymbol{\theta}}^T \mathbf{p} - L(\boldsymbol{\theta}, \dot{\boldsymbol{\theta}})$.

be factorised in the form $[N(\Theta)]^T[N(\Theta)]$ with $[N(\Theta)]$ integrable. In such a situation, the Hamilton's equation can be written as

$$\begin{aligned}\dot{\Theta} &= \mathbf{P} \\ \dot{\mathbf{P}} &= [N(\Theta)]^{-T}\Gamma\end{aligned}\tag{10}$$

For inertial motions $\Gamma = 0$, and we can integrate the equations(10). Since we can integrate the equations explicitly such systems cannot exhibit chaos. Hence we can conclude that *if the symbols R_{ijkl} vanish identically for any manipulator, then, for inertial motions, such manipulators cannot exhibit chaotic motions.*

Next we consider the case when one or more of the R_{ijkl} are non-zero. In such cases, we can calculate the Gaussian curvature, G , of the 2D subspaces of the full configuration space with metric tensor $[M(\boldsymbol{\theta})]$. The Gaussian curvature, in terms of the metric coefficients M_{ij} , $i, j = 1, 2$, for any 2D subspace is given by ²

$$G = \frac{1}{M_{11}M_{22} - M_{12}^2} \left(\frac{\partial^2 M_{12}}{\partial\theta_1\partial\theta_2} - \frac{1}{2} \frac{\partial^2 M_{11}}{\partial\theta_2^2} - \frac{1}{2} \frac{\partial^2 M_{22}}{\partial\theta_1^2} + \sum_{\gamma,\delta=1}^2 \Gamma_{12}^\gamma \Gamma_{12}^\delta M_{\gamma\delta} - \sum_{\alpha,\beta=1}^2 \Gamma_{11}^\alpha \Gamma_{22}^\beta M_{\alpha\beta} \right)\tag{11}$$

where the Christoffel symbols, Γ_{ij}^l , are defined in equation(7).

If G is identically zero for all 2D subspaces, then it is equivalent to all the R_{ijkl} vanishing identically and we cannot have chaos. Hence we consider the cases $G > 0$ and $G < 0$ in a 2D subspace of the configuration space. Figure 1 show sketches of two surfaces with G less than and greater than zero respectively³. In the absence of external forces, the motion of the system from any initial state will take place along the geodesic of the surface(Arnold 1989). For surfaces with $G < 0$, the geodesics diverge (as shown schematically in figure 1). If two states are initially separated by a distance ϵ_0 , over time the distance between the two trajectories will grow exponentially as

$$\epsilon(t) = \epsilon_0 e^{\sqrt{-G}t}\tag{12}$$

Hence however small is the initial distance ϵ_0 , the distance between two trajectories, $\epsilon(t)$, tends to infinity as time increases for surfaces with $G < 0$. Such sensitive dependence on initial condition is the hallmark of chaos and this has been termed as kinematic source of chaos(Zak 1985a; Zak 1985b) since there is no external forcing in this analysis. It maybe mentioned that if $G > 0$ then initially nearby trajectories do not diverge and hence the inertial motion is not chaotic(see figure 1).

From the above, we can conclude that *if $G < 0$ in any 2D subspace of the configuration space of a manipulator, then, for inertial motions, the manipulator can exhibit chaos.*

² G can also be written in terms of the symbols R_{ijkl} (Stoker 1969).

³Surfaces with $G > 0$ are analogous to a *sphere* and surfaces with $G < 0$ are called *pseudo-spheres*.

Our analytical criteria is based on the above conclusion and in the next section, we calculate the Gaussian curvature for several two and three-degree-of-freedom robots and develop conditions for which the robots can exhibit chaotic motions.

Before we compute the Gaussian curvatures, a word about non-inertial or forced motion is in order since the input control torque in a robot clearly makes the motion forced. For non-inertial or forced motions, the motion *doesn't* take place along the geodesics of the surface. The motion is determined by the underlying surface (or manifold) characterised by the Gaussian (or Riemannian) curvature and the acceleration or external force characterised by the *geodesic* curvature. Hence the analytical criteria developed above may not hold for externally forced motions⁴. For study of forced motions we resort to the well known tools in the study of chaos and these will be described in a later section.

4 Gaussian curvature of two and three-degree-of-freedom robots

In this section, we derive the general expressions of Gaussian curvature of several two and three-degree-of-freedom robots containing prismatic(P) and revolute(R) joints. From these expressions and the criteria described in the last section, we infer whether such robots can exhibit chaotic motions in the absence of compliance, friction and potential energy (gravity terms in our case).

4.1 The PP robot

Figure 2 shows a two-degree-of-freedom robot with two prismatic (P) joints. The translations at the joints are denoted by d_1 and d_2 and the masses of the two links are m_1 and m_2 . The kinetic energy of the PP robot in terms of the velocities at the joints and the masses can be written as

$$KE = \frac{1}{2}m_1\dot{d}_1^2 + \frac{1}{2}m_2\dot{d}_2^2 \quad (13)$$

The element of the mass matrix are constants and are given as

$$\begin{aligned} M_{11} &= m_1 \\ M_{12} &= 0 \\ M_{22} &= m_2 \end{aligned} \quad (14)$$

The Christoffel symbols are zero since the metric tensor $[M(\boldsymbol{\theta})]$ has constant coefficients. The Gaussian curvature is zero and hence a PP robot cannot exhibit chaos when there is no external force. This result is expected since the differential equations describing the

⁴In the case of the PR robot (discussed later), the Gaussian curvature is zero and hence the PR robot *does not* have a kinematic source of chaos. We were also not able to observe chaotic motions in the *forced case* inspite of extensive numerical simulations.

dynamics of a PP robot are *linear* and it is well known that linear systems *do not* exhibit chaos.

4.2 The PR robot

Figure 3 shows a two-degree-of-freedom robot containing a prismatic(P) and a revolute(R) joint. The kinetic energy of the PR robot can be written as

$$KE = \frac{1}{2}(m_1 + m_2)\dot{d}_1^2 + \frac{1}{2}(m_2r_2^2 + I_2)\dot{\theta}_2^2 - m_2r_2\dot{d}_1\dot{\theta}_2 \sin \theta_2 \quad (15)$$

where m_1 is the mass of link 1, m_2, I_2, r_2 are the mass, inertia and location of the center of gravity of link 2, and d_1, θ_2 are two joint variables.

The elements of the mass matrix are given by

$$\begin{aligned} M_{11} &= m_1 + m_2 \\ M_{12} &= -m_2r_2 \sin \theta_2 \\ M_{22} &= m_2r_2^2 + I_2 \end{aligned} \quad (16)$$

The Christoffel symbols $\Gamma_{11}^1, \Gamma_{11}^2, \Gamma_{12}^1$ and Γ_{12}^2 are zero and the non-zero ones are given as

$$\begin{aligned} \Gamma_{22}^1 &= -\frac{m_2r_2 \cos \theta_2 M_{22}}{M^2} \\ \Gamma_{22}^2 &= \frac{m_2r_2 \cos \theta_2 M_{12}}{M^2} \end{aligned} \quad (17)$$

where $M^2 = M_{11}M_{22} - M_{12}^2$.

Substituting the above expressions into equation(11) we obtain the Gaussian curvature of the PR robot to be zero. For the PR robot, one can factorise the mass matrix and get

$$[N(\theta_2)] = \begin{bmatrix} \frac{M_{12}}{\sqrt{M_{22}}} & \sqrt{M_{22}} \\ \sqrt{M_{11} - \frac{M_{12}^2}{M_{22}}} & 0 \end{bmatrix} \quad (18)$$

where the symbols M_{ij} are given in equations (16). The equation of motions of an unforced PR robot can be integrated in the closed form and hence the unforced PR robot does not have a kinematic source of chaos.

4.3 The RP robot

The kinetic energy of the RP robot moving in a horizontal plane as shown in figure 4 can be written as

$$KE = \frac{1}{2}(I + m_2d_2^2)\dot{\theta}_1^2 + \frac{1}{2}m_2\dot{d}_2^2 \quad (19)$$

where θ_1 and d_2 are the joint variables, m_2 is the mass of link 2, and I is sum of the inertias given by $I_1 + I_2 + m_1 r_1^2$ with r_1 as the distance to the centre of mass of link 1.

The elements of the mass matrix are

$$\begin{aligned} M_{11} &= I + m_2 d_2^2 \\ M_{12} &= 0 \\ M_{22} &= m_2 \end{aligned} \tag{20}$$

The Christoffel symbols Γ_{12}^2 , Γ_{22}^1 and Γ_{22}^2 are zero and the rest are given as

$$\begin{aligned} \Gamma_{11}^2 &= \frac{-m_2 d_2 M_{11}}{M^2} \\ \Gamma_{12}^1 &= \frac{m_2 d_2 M_{22}}{M^2} \end{aligned} \tag{21}$$

The expression for the Gaussian curvature is

$$G = \frac{1}{M^2} \left[-m_2 + \left(\frac{m_2 d_2 M_{22}}{M^2} \right)^2 M_{11} \right] \tag{22}$$

where $M^2 = M_{11} M_{22} - M_{12}^2$.

One can show that for positive I , G is less than zero, and the RP robot has kinematic sources of chaos. The proof is as follows:

Assume $G \geq 0$. Then we have

$$\begin{aligned} \left[\left(\frac{m_2 d_2 M_{22}}{M^2} \right)^2 M_{11} \right] - m_2 &\geq 0 \\ \text{or } m_2 d_2^2 M_{11} &\geq M_{11}^2, \\ \text{or } m_2 d_2^2 &\geq M_{11}. \end{aligned}$$

For $I > 0$ this is false from equations(20), hence $G < 0$.

4.4 The RR robot

The kinetic energy of the RR robot moving on a horizontal plane as shown in figure 5 can be written as

$$KE = (c_1 + c_2 \cos \theta_2) \dot{\theta}_1^2 + (c_3 + c_4 \cos \theta_2) \dot{\theta}_1 \dot{\theta}_2 + c_3 \dot{\theta}_2^2 \tag{23}$$

where the constants c_i are given as

$$\begin{aligned} c_1 &= m_1 r_1^2 + I_1 + I_2 + m_2 r_2^2 + m_2 l_1^2 \\ c_2 &= 2m_2 l_1 r_2 \\ c_3 &= m_2 r_2^2 + I_2 \\ c_4 &= m_2 l_1 r_2 \end{aligned}$$

with θ_i , $i = 1, 2$ denoting the joint variables, m_i, I_i, r_i , $i = 1, 2$ denoting the mass, inertia and location of the center of gravity of link i respectively, and l_1 denoting the length of link 1.

The elements of the mass matrix are

$$\begin{aligned} M_{11} &= c_1 + c_2 \cos \theta_2 \\ M_{12} &= 2(c_3 + c_4 \cos \theta_2) \\ M_{22} &= c_3 \end{aligned} \quad (24)$$

The expressions for Γ_{ij}^k and the Gaussian curvature G are given as

$$\begin{aligned} \Gamma_{11}^1 &= \frac{-c_2 \sin \theta_2 M_{12}}{2M^2}, \quad \Gamma_{11}^2 = \frac{c_2 \sin \theta_2 M_{11}}{2M^2}, \quad \Gamma_{22}^1 = \frac{-4c_4 \sin \theta_2 M_{22}}{2M^2} \\ \Gamma_{22}^2 &= \frac{4c_4 \sin \theta_2 M_{22}}{2M^2}, \quad \Gamma_{12}^1 = \frac{c_2 \sin \theta_2 M_{12}}{2M^2}, \quad \Gamma_{12}^2 = \frac{-c_2 \sin \theta_2 M_{12}}{2M^2} \\ G &= \frac{1}{M^2} \left(\frac{c_2 \cos \theta_2}{2} + \left(\frac{\sin \theta_2}{2M^2} \right)^2 \left(M_{11}^3 c_2^2 - 2c_2^2 M_{11} M_{12}^2 + c_2^2 M_{12} M_{22} - 4c_4 c_2 M_{11}^2 M_{22} - M_{12}^2 \right) \right) \end{aligned} \quad (25)$$

where $M^2 = M_{11}M_{22} - M_{12}^2$.

The Gaussian curvature is negative when

$$\cos \theta_2 < -\frac{a_2 c_1 - b_1 + 2a_3 c_3 - a_4 c_1 + 2a_5 c_3}{a_1 + a_2 c_2 + 2a_3 c_4 - a_4 c_2 + 2a_5 c_4} \quad (26)$$

where the symbols a_1, a_2, a_3, a_4, a_5 and b_1 are given by $(1/2)c_2, \beta^2 c_2 M_{11}^2, 4\beta^2 c_2 c_4 M_{12}^2, 2\beta^2 c_2^2 M_{12}^2, \beta^2 c_2^2 c_5$, and $4c_4 c_5 M_{11} \beta^2 c_2$ respectively with $\beta = \sin \theta_2 / (M_{11}M_{22} - M_{12}^2)$. The Gaussian curvature of the unforced RR robot can be negative and hence the the unforced RR robot can exhibit chaos.

4.5 The RRR robot

Figure 6 shows a three-degree-of-freedom robot with all revolute(R) joints. In terms of the kinematic and inertial parameters, the kinetic energy of the RRR robot is given as

$$KE = \frac{1}{2} \left(M_{11} \dot{\theta}_1^2 + M_{22} \dot{\theta}_2^2 + M_{33} \dot{\theta}_3^2 + 2M_{12} \dot{\theta}_1 \dot{\theta}_2 + 2M_{23} \dot{\theta}_2 \dot{\theta}_3 + 2M_{13} \dot{\theta}_1 \dot{\theta}_3 \right) \quad (27)$$

where θ_i , $i = 1, 2, 3$, are the three joint variables and the elements of the mass matrix are

$$\begin{aligned} M_{11} &= I_1 + I_3 \cos^2 \theta_2 + I_7 \sin^2(\theta_2 + \theta_3) + I_{11} \sin \theta_2 \cos \theta_2 + I_3 \cos \theta_2 \sin(\theta_2 + \theta_3) \\ M_{12} &= I_4 \sin \theta_2 + I_8 \cos(\theta_2 + \theta_3) + I_9 \cos \theta_2 \\ M_{13} &= I_8 \cos(\theta_2 + \theta_3) \\ M_{22} &= 2I_5 \sin \theta_3 + I_2 + I_6 \\ M_{23} &= I_5 \sin \theta_3 + I_6 \\ M_{33} &= I_6 \end{aligned} \quad (28)$$

In the above equation, the symbols I_i 's are constants dependent on the lengths, masses and inertia of the links and are given in (Armstrong, Khatib and Burdick 1986). The configuration space for the RRR robot is 3 dimensional and three Gaussian curvatures of the 2D subspaces are

$$\begin{aligned}
G_{12} &= \frac{1}{M_{11}M_{22} - M_{12}^2} \left[\frac{I_3 \cos(2\theta_2)}{2} - \frac{I_7 \cos(\theta_2 + \theta_3)}{2} + I_{11} \sin(2\theta_2) - 2I_3 \sin(2\theta_2 + \theta_3) \right. \\
&\quad + \frac{1}{4(M_{11}M_{22} - M_{12}^2)} [(-I_3 \sin(2\theta_2) + I_7 \sin 2(\theta_2 + \theta_3) + I_{11} \cos(2\theta_2) + \\
&\quad 2I_3 \cos(2\theta_2 + \theta_3))^2 M_{22} - ((-I_3 \sin(2\theta_2) + I_7 \sin 2(\theta_2 + \theta_3) + I_{11} \cos(2\theta_2) + \\
&\quad 2I_3 \cos(2\theta_2 + \theta_3))(I_4 \cos \theta_2 - I_8 \sin(\theta_2 + \theta_3) - I_9 \sin(\theta_2))] M_{12}] \\
G_{13} &= \frac{1}{M_{11}M_{33} - M_{13}^2} [I_3 \cos(\theta_2) \sin(\theta_2 + \theta_3) - I_7 \cos(\theta_2 + \theta_3) \\
&\quad + \frac{M_{33}}{M_{11}M_{33} - M_{13}^2} (I_7 \cos(\theta_2 + \theta_3) \sin(\theta_2 + \theta_3) + I_3 \cos \theta_2 \cos(\theta_2 + \theta_3))^2 - \\
&\quad \frac{I_8 \sin(\theta_2 + \theta_3)}{(M_{11}M_{33} - M_{13}^2)^2} \left(\frac{M_{12}}{2} (-I_3 \sin(2\theta_2) + I_7 \sin 2(\theta_2 + \theta_3) + \right. \\
&\quad I_{11} \cos(2\theta_2) + 2I_3 \cos(2\theta_2 + \theta_3)) (M_{13}^2 - M_{11}M_{22}) + (I_7 \cos(\theta_2 + \theta_3) \sin(\theta_2 + \theta_3) + \\
&\quad \left. I_3 \cos \theta_2 \cos(\theta_2 + \theta_3)) M_{13}^2 (M_{33} - M_{22}) \right] \\
G_{23} &= (2 - e)\alpha - b\alpha^2 - d - 4I_5
\end{aligned}$$

where

$$\begin{aligned}
\alpha &= \sin \theta_3 \\
e &= \frac{28I_5^2 \cos^2 \theta_3}{M_{22}M_{33} - M_{23}^2} I_5 I_6^2 + I_2 I_5 I_6 \\
b &= \frac{4I_5^2 \cos^2 \theta_3}{3I_5^2 I_6} \\
d &= 2I_2 I_6^2 + 3I_6^2
\end{aligned}$$

The sign of G_{23} is negative when $e\alpha > 2\alpha - b\alpha^2 - d - 4I_5$, however, it is difficult to infer under what conditions the sign of G_{12} and G_{13} are negative. In any case, the RRR robot can exhibit chaos since G_{23} can be negative.

4.6 The RRP robot

Figure 7 shows a three-degree-of-freedom RRP robot. In terms of the kinematic and inertial parameters, the kinetic energy of the RRP robot is given as

$$KE = \frac{1}{2} \left(M_{11} \dot{\theta}_1^2 + M_{22} \dot{\theta}_2^2 + M_{33} \dot{d}_3^2 + 2M_{12} \dot{\theta}_1 \dot{\theta}_2 + 2M_{23} \dot{\theta}_2 \dot{d}_3 + 2M_{13} \dot{\theta}_1 \dot{d}_3 \right)$$

where $\theta_i, i = 1, 2$, and d_3 are the three joint variables, and the elements of the mass matrix are

$$\begin{aligned}
M_{11} &= K_1 + \sin^2 \theta_2 (K_2 + K_3 d_3 + K_{10} d_3^2) \\
M_{12} &= -K_7 \cos \theta_2 d_3 \\
M_{13} &= -K_8 \sin \theta_2 \\
M_{22} &= K_4 + K_5 d_3 + K_6 d_3^2 \\
M_{23} &= 0 \\
M_{33} &= K_9
\end{aligned}$$

where the symbols K_i are constants given by

$$\begin{aligned}
K_1 &= m_1 k_{1yy}^2 + m_2 k_{2xx}^2 + 2m_2 y_2 d_2 + d_2^2 (m_2 + m_3) \\
K_2 &= m_3 k_{3xx}^2 \\
K_3 &= K_5 = 2m_3 z_3 \\
K_4 &= m_2 k_{2yy}^2 + m_3 k_{3yy}^2 \\
K_6 &= K_9 = K_{10} = m_3 \\
K_7 &= K_8 = -m_3 d_2
\end{aligned}$$

where $m_{(\cdot)}, k_{(\cdot)}, d_2, z_3$ are the masses, inertias and lengths respectively associated with the links (Paul 1981).

The configuration space for the RRP robot is 3 dimensional and the expressions for the three Gaussian curvatures of the 2D subspaces are

$$\begin{aligned}
G_{12} &= \frac{1}{M_{11}M_{22} - M_{12}^2} \left\{ (-K_2 - K_3 d_3) \cos(2\theta_2) + \frac{(K_2 + K_3 d_3 + K_{10} d_3^2) M_{22} \sin^2 2\theta_2}{4(M_{11}M_{22} - M_{12}^2)^2} \right. \\
&\quad \left. \left[(K_2 + K_3 d_3 + K_{10} d_3^2) M_{22} M_{11} - (2 + K_2 + K_3 d_3 + K_{10} d_3^2) M_{21}^2 \right] \right. \\
&\quad \left. - \frac{(K_2 + K_3 d_3 + K_{10} d_3^2) (K_7 d_3 \sin \theta_2) (M_{13}^2 - 2M_{12}M_{11} - M_{11}M_{22}M_{21})}{4(M_{11}M_{22} - M_{12}^2)^2} \right\} \\
G_{23} &= (K_5 + 2K_6 d_3)^2 K_9^2 - M_{22} K_6 \\
G_{31} &= 2(-K_8 \sin \theta_2) + K_1 + \sin^2 \theta_2 (K_2 + K_3 + K_{10} d_3^2)
\end{aligned}$$

For the RRP robot, for all positive values of K_1 , G_{31} is positive. However, G_{23} can be negative, if $M_{22} K_6 > (K_5 + 2K_6 d_3)^2 K_9^2$ and the RRP robot can exhibit chaos.

5 Numerical study of robot control equations

As mentioned before, the equations of motion inclusive of the control torques cannot be analysed using the criteria of Gaussian curvature alone. To study them we resort to numerical

integration and use the several well known diagnostic criteria for chaos. The main diagnostic criteria for chaos are phase plots, Poincaré maps, Lyapunov exponents and bifurcation diagrams (Moon 1987). In this section, we first briefly discuss these criteria, then present the equations of motion of a feedback controlled RP and RR robot in a form amenable for numerical study, and finally present some numerical results. We chose the RP and the RR robots since these have negative Gaussian curvatures and the state equations are 4 dimensional. The state equations of the RRR and RRP robots are 6 dimensional and require significantly more computation and hence were not chosen for simulations. The feedback controlled PP and PR robot didn't exhibit chaotic motions even after extensive searches in the absence of friction and potential energy.

5.1 Diagnostic criteria for chaos

Phase plots are plots of state velocity versus state position. For a periodic input, the phase plots of a non-chaotic system are closed and have one or more but finite number of periods or loops. In the case of a chaotic system, the phase plots is not closed and there are infinite number of periods or loops. The phase trajectories tends to fill up a certain region of the phase space.

A section transverse to the flow in the phase space of an n dimensional continuous system is an $n-1$ dimensional map called the Poincaré map. For a system, driven by a periodic input of period T , the Poincaré sections can be defined by the planes $t = iT$ where, $i = 1, 2, 3, \dots$ and can be pictured as a stroboscopic sampling of the velocity and position at every time period T . For a non-chaotic system, the Poincaré section contains one or more but finite number of points. For a chaotic system, the Poincaré map fills up a bounded region region and has fractal dimension. This is also called the strange attractor.

However, the most important and useful tool to identify chaos are the Lyapunov exponents. The Lyapunov exponent is a measure of the average long-term exponential rate of divergence of all adjacent trajectories as $t \rightarrow \infty$. For an n dimensional system, there are n Lyapunov exponents and one or more positive Lyapunov exponent with a bounded attractor indicates chaotic motion. The algorithm given by Wolf et al.(Wolf, Swift, Swinney and Vastano 1985) to compute the Lyapunov exponents has been widely used to determine the Lyapunov exponents and in this paper we use the same algorithm.

Once a system is found to be chaotic, bifurcation diagrams are used to study the pre-chaotic or post-chaotic behavior as a critical parameter is varied. Bifurcation diagrams describes the nature of transition from periodic motion to chaos, as the parameter is varied, enables one to anticipate chaotic behavior and to indicate the route to chaos. Bifurcation diagrams can be obtained by the geometric approach of Kawakami(Kawakami 1984), continuation methods or the brute force approach(Parker and Chua 1989). In this paper, we have computed the bifurcation diagrams by the brute force method.

5.2 The planar RP robot under feedback control

Figure 4 shows the RP robot. Neglecting compliance and friction at the joints, the equations of motion of a RP robot, moving in a horizontal plane, can be written as

$$\begin{aligned} (m_1 l_1^2 + I_1 + I_2 + m_2 d_2^2) \ddot{\theta}_1 + 2m_2 d_2 \dot{\theta}_1 \dot{d}_2 &= \Gamma_1 \\ m_2 \ddot{d}_2 - m_2 d_2 \dot{\theta}_1^2 &= F_2 \end{aligned} \quad (29)$$

where, m_i , l_i , I_i and denote the mass, position of the center of mass of link i , and inertia of link i respectively. We use the following non-dimensional parameters:

$$\begin{aligned} \rho_1 &= \left(1 + \frac{I_1 + I_2}{m_1 l_1^2}\right), & \rho_2 &= \frac{m_2}{m_1} \\ \rho_3 &= \frac{m_1 l_1^2 \text{ kgm}^2}{1.0 \text{ kgm}^2}, & \rho_4 &= \frac{m_1 l_1 \text{ kgm}}{1.0 \text{ kgm}} \\ X &= \frac{d_2}{l_1} \\ \Gamma_1^* &= \frac{\Gamma_1}{\rho_3}, & F_2^* &= \frac{F_2}{\rho_4} \end{aligned} \quad (30)$$

and consider the two control laws described in section 2, namely, (i) proportional plus derivative (PD) control scheme and (ii) model based control. Although, in general, there are two proportional and two derivative gains, to restrict the parametric plane we choose both of them to be equal and denote them as K_p and K_v . Using the normalised time, $\tau = \omega t$, and the normalised gains,

$$\begin{aligned} K_p^* &= K_p / \omega^2 \\ K_v^* &= K_v / \omega \end{aligned} \quad (31)$$

we can, after simplification get a system of 4 first order coupled, nonlinear and autonomous ordinary differential equations. These are the PD control equations of a planar RP robot and are given as

$$\begin{aligned} &\begin{bmatrix} \rho_1 + \rho_2 X^2 & 0 \\ 0 & \rho_2 \end{bmatrix} \begin{bmatrix} \theta_1'' \\ X'' \end{bmatrix} \\ &= \begin{bmatrix} \frac{1}{\rho_3} [K_p^* (A_1 \sin \tau - \theta_1) + K_v^* (A_1 \cos \tau - \theta_1') + \theta_{1d}''] \\ \frac{1}{\rho_4} [K_p^* (A_2 \sin \tau - X) + K_v^* (A_2 \cos \tau - X') + X_d''] \end{bmatrix} \end{aligned} \quad (32)$$

where $(\cdot)'$ denotes derivative with respect to non-dimensional time τ .

In the model based control scheme joint torques are calculated, as described in section 2. The quantities $\widehat{\mathbf{M}}(\boldsymbol{\theta})$ and $\widehat{\mathbf{C}}(\boldsymbol{\theta}, \dot{\boldsymbol{\theta}})$ are the estimated mass matrix and centrifugal and Coriolis torques vector which are computed by perturbing the non-dimensional parameters as

$$\begin{aligned} \hat{\rho}_1 &= (1 + \epsilon) \rho_1 \\ \hat{\rho}_2 &= (1 + \epsilon) \rho_2 \end{aligned} \quad (33)$$

The model based control equations for a RP robot in terms of the non-dimensional parameters are

$$\begin{aligned}
(\rho_1 + \rho_2 X^2) \theta_1'' &= (\rho_1 + \rho_2 X^2)(1 + \epsilon)[K_p^*(A_1 \sin \tau - \theta_1) + K_v^*(A_1 \cos \tau - \theta_1') + \theta_{1d}''] \\
&\quad - 2\rho_2 \epsilon X \theta_1' X' \\
X'' &= (1 + \epsilon)[K_p^*(A_2 \sin \tau - X) + K_v^*(A_2 \cos \tau - X') + X_d''] - \epsilon X \theta_1'^2 \quad (34)
\end{aligned}$$

The above non-dimensional equations (32) and (34) were used for the numerical simulations and were more helpful in systematically obtaining values of length and inertial parameters for which the RP robot exhibits chaotic motions.

5.3 The planar RR robot under feedback control

Figure 5 show a two-degree-of-freedom RR robot. Similar to the RP robot above, the equations of motion of a planar 2R robot can be derived in the non-dimensional form with the introduction of the following non-dimensional variables:

$$\begin{aligned}
\rho_I &= \frac{m_1 r_1^2 + I_1}{m_2 r_2^2 + I_2} \\
\rho_{II} &= \frac{m_1 l_1^2}{m_2 r_2^2 + I_2} \\
\rho_r &= \frac{r_2}{l_1} \\
\rho_{k_p} &= \frac{K_p}{\omega^2 (m_2 r_2^2 + I_2)} \\
\rho_{k_v} &= \frac{K_v}{\omega (m_2 r_2^2 + I_2)}
\end{aligned} \quad (35)$$

The equations of the robot under PD control, using the above non-dimensional variables, can be written as

$$\begin{aligned}
&\begin{bmatrix} \rho_I + 1 + \rho_{II}(1 + 2\rho_r \cos \theta_2) & 1 + \rho_{II}\rho_r \cos \theta_2 \\ 1 + \rho_{II}\rho_r \cos \theta_2 & 1 \end{bmatrix} \begin{bmatrix} \theta_1'' \\ \theta_2'' \end{bmatrix} \\
&+ \begin{bmatrix} -\rho_{II}\rho_r \sin \theta_2 (2\theta_1' + \theta_2') \theta_2' & 0 \\ 0 & \rho_{II}\rho_r \theta_1'^2 \sin \theta_2 \end{bmatrix} \\
&= \begin{bmatrix} \rho_{k_p}(\theta_1 - A_1 \sin \tau) + \rho_{k_v}(\theta_1' - A_1 \cos \tau) \\ \rho_{k_p}(\theta_2 - A_2 \sin \tau) + \rho_{k_v}(\theta_2' - A_2 \cos \tau) \end{bmatrix} \quad (36)
\end{aligned}$$

where, $(\cdot)'$ denotes derivative with respect to τ .

The RR robot equations under model based control can be written as

$$\begin{aligned}
& \begin{bmatrix} \rho_I + 1 + \rho_{II}(1 + 2\rho_r \cos \theta_2) & 1 + \rho_{II}\rho_r \cos \theta_2 \\ 1 + \rho_{II}\rho_r \cos \theta_2 & 1 \end{bmatrix} \begin{bmatrix} \theta_1'' \\ \theta_2'' \end{bmatrix} \\
& + \begin{bmatrix} -\rho_{II}\rho_r \sin \theta_2(2\theta_1' + \theta_2')\theta_2' & 0 \\ 0 & \rho_{II}\rho_r\theta_1'^2 \sin \theta_2 \end{bmatrix} \\
& = \begin{bmatrix} \alpha_I \{-A_1 \sin \tau + K_v^*(\theta_1' - A_1 \cos \tau) + K_p^*(\theta_1 - A_1 \sin \tau)\} + \alpha_{II} \{-2(A_1 + A_2) \\ \cos \theta_2 \sin \tau + \sin \tau(\theta_1' + \theta_2')\theta_2' + K_v^* \cos \theta_2 [2(\theta_1' - A_1 \cos \tau) + \\ (\theta_2' - A_2 \cos \tau)] + K_p^* \cos \theta_2 [2(\theta_1 - A_1 \sin \tau) + (\theta_2 - A_2 \sin \tau)]\} + \alpha_{III} \{-A_2 \sin \tau \\ + K_v^*(\theta_2' - A_2 \cos \tau) + K_p^*(\theta_2 - A_2 \sin \tau)\} \\ \alpha_{III} \{-(A_1 + A_2) \sin \tau + K_v^*[\theta_1' - A_1 \cos \tau + \theta_2' - A_2 \cos \tau] + K_p^*[\theta_1 \\ - A_1 \sin \tau + \theta_2 - A_2 \sin \tau]\} + \alpha_{II} \{-\sin \tau [A_1 \cos \theta_2 + \theta_1'^2] + K_v^* \cos \theta_2 [\theta_1' \\ - A_1 \cos \tau] + K_p^* \cos \theta_2 [\theta_1 - A_1 \sin \tau]\} \end{bmatrix} \quad (37)
\end{aligned}$$

where, in addition to the non-dimensional variables defined for the PD case, we have five additional variables defined by

$$\begin{aligned}
\alpha_I &= \frac{\hat{m}_1 \hat{r}_1^2 + \hat{I}_1 + \hat{m}_2 \hat{r}_2^2 + \hat{I}_2 + \hat{m}_2 \hat{l}_1^2}{m_2 r_2^2 + I_2} \\
\alpha_{II} &= \frac{\hat{m}_2 \hat{l}_1 \hat{r}_2}{m_2 r_2^2 + I_2} \\
\alpha_{III} &= \frac{\hat{m}_2 \hat{r}_2^2 + \hat{I}_2}{m_2 r_2^2 + I_2} \\
K_v^* &= \frac{K_v}{\omega} \\
K_p^* &= \frac{K_p}{\omega^2}
\end{aligned}$$

where $\widehat{(\cdot)}$ denote the estimated quantities obtained in a manner similar to the RP robot.

5.4 Numerical results

The equations of motion for the RP and RR robots under feedback control were numerical integrated using a variable step, variable order, predictor corrector Adams algorithm(Gordon

and Shampine 1975). In order to ensure that the numerical results were not an artifact of the numerical integration scheme, the results were verified with Runge-Kutta 4-5 integration routine. The results were also checked for relative and absolute error tolerances of 10^{-6} and 10^{-9} . The numerical work was done on Sun Sparc10 and IBM RS 6000 workstations. A large number of values of the non-dimensional parameters were tried in our numerical study. In this paper we present results for only one set of values for the RP and the RR robot.

For the RP robot, the amplitude of the repetitive motion are assumed to be π radians for θ_1 and 1.0 for X . The frequency ω was assumed to be 1.0rad/sec. The non-dimensional parameters of the RP robot were chosen as $\rho_1 = 2.5$, $\rho_2 = 0.5$, $\rho_3 = 0.4$ and $\rho_4 = 2.0$ and the equations of motion of the RP robot under feedback control were numerically integrated with various initial conditions. After an initial transient period, the global behavior of the trajectory was found to be similar. Figure 8 and 9 shows phase plots for typical non-chaotic and chaotic cases for the PD controlled RP robot where we plot the non-dimensional variable X given by d_2/l_1 and its derivative \dot{X} . It can be seen that, in the non-chaotic case the trajectory settles to a limit cycle, whereas in the chaotic case the trajectory moves around in a bounded region of the phase space. It may be noted that these phase plots are a projection of the actual trajectory in \mathfrak{R}^4 phase space.

A typical plot of the largest Lyapunov exponent for RP robot with chaotic parameters is shown in figure 10, and figure 11 shows the time evolution for non-chaotic parameters. It can be seen that Lyapunov exponent is positive for the chaotic case and negative for the non-chaotic case.

Figure 12 shows the Poincaré map for a set of chaotic parameters. This map was obtained by sampling the results of numerical integration at intervals of forcing period i.e., 2π . The resultant map is in \mathfrak{R}^4 space and only the $(\theta_1, \dot{\theta}_1)$ projection is shown in figure 12 where θ_1 is in radians and $\dot{\theta}_1$ is in rad/sec.

We performed a search of the (K_p^*, K_v^*) space for the RP robot by varying K_p^* in steps of 1.0 and K_v^* in steps of 0.1. Figures 13 and 14 shows the values of K_p^* and K_v^* for which the largest Lyapunov exponent is positive for the PD and model based control respectively. These chaos maps shows the values of gains for which the RP robot control equations show chaotic behavior. The initial conditions (0 radians, 0, π rad/sec, 1.0) for $\theta_1, X, \dot{\theta}_1, \dot{X}$ respectively were used to obtain the chaos maps.

Figures 15, 16 show bifurcation diagrams corresponding to one range of parameter ($K_v^* = 0.5$). As the parameter K_p^* is varied the response changes from periodic to chaotic motion. The period doubling phenomenon can be seen in these figures. In figure 15 θ is in radians and X in figure 16 is the non-dimensional number d_2/l_1 .

Similar to the RP robot above, we performed similar numerical study for the RR manipulator. The non-dimensional parameters for the RR robot were obtained from the inertial parameters of the first two links of the CMU DD arm II(Khosla 1986). These are given by $\rho_I = 3.1637$, $\rho_{II} = 0.9385$, $\rho_r = 0.52$, $\alpha_I = 0.9146$, $\alpha_{II} = 0.01952$, and $\alpha_{III} = 0.1513$. The amplitude of the repetitive motion was chosen as $\pi/2$ radians and $\pi/4$ radians for θ_1 and θ_2 respectively. The forcing frequency was assumed to be 2.0 rad/sec.

Figures 17 show the typical Lyapunov exponents for the RR robot for the PD and the model based control respectively. We conducted a search of the (K_p, K_v) space for values of gains which give positive Lyapunov exponent. Figure 18 gives the values of the controller gains for the RR robot under PD control which give chaotic motions. Figure 19 shows the values of the gains in the case of a model based control with a large underestimation of $\epsilon = -0.9$. To obtain the chaos maps, we have used the initial conditions $(0, \pi, 0, \pi/2)$ for $\theta_1, \dot{\theta}_1, \theta_2, \dot{\theta}_2$ respectively.

We have obtained such chaos maps for several values of underestimations and it was observed that the region of chaos was larger when the underestimation is larger. For small amounts of underestimations (less than 50%), there are no values of (K_p, K_v) which give positive Lyapunov exponents.

Figure 20 shows the bifurcation diagram for θ_2 for the RR robot with model based control for $\epsilon = -0.9$ and $K_p = 49$. It clearly shows a period doubling route to chaos. The period doubling phenomenon was observed for several other values of gains and underestimations.

6 Conclusion

In this paper, we have explored the possibility of chaotic motions in two and three-degree-of-freedom, serial, rigid robots containing revolute(R) and prismatic(P) joints under feedback control. We presented an analytical criteria, based on the concept of Gaussian and Riemannian curvature, which can be used to predict chaos in the case of unforced motion of the robots in the absence of compliance, friction and potential energy. For the forced motion, we present numerical simulation results for the two-degree-of-freedom RP and RR robots. From the analytical and numerical study we make the following major conclusions:

- The Gaussian curvature of the configuration space of the PP and the PR robot with the mass matrix as the metric is zero. Hence, the PP and the PR robot cannot have kinematic source of chaos. The equations of motion, without any forcing, can be integrated in closed form for both the robots.
- The Gaussian curvature of the configuration space of the RP and the RR robot with the mass matrix as the metric can be negative. Hence the inertial motions of a RP and the RR robot can exhibit chaos. For the three-degree-of-freedom RRR and RRP robots there exists values of mass, length and inertia for which the Gaussian curvatures of the 2D subspaces are negative and hence these robots can also exhibit chaos.
- In case of the forced motion, the RP and RR robots can exhibit chaotic motions for a simple PD controller and for a model based controller with mismatch in model parameters. However, inspite of extensive numerical experiments, the PR manipulator did not exhibit chaos with either the PD or the model based controller. The existence of chaotic motions were verified by careful numerical simulations and by use of the largest Lyapunov exponent.

- Chaotic motions are more likely to occur for small values of derivative gains and for large mismatch between the dynamic model and the actual robot parameters in case of model based control. It is more easily seen for underestimated models.
- The route to chaos appears to be through period doubling.

The study apart from mathematical interest can serve as a tool in the design and analysis of actual robot controllers. The study can also help in obtaining conditions for better trajectory tracking in feedback controlled actual robots in the presence of friction and potential energy.

7 Acknowledgement

The programs for numerical study of chaotic motions were developed in part by L. Shrinivas and we gratefully acknowledge his help. The authors also thank the anonymous reviewers for their helpful comments.

References

- Armstrong, B., Khatib, O. and Burdick, J. W. (1986), The explicit dynamic model and inertial parameters of the puma 560 arm, *in* 'International Conference on Robotics and Automation', pp. 510–517.
- Arnold, V. I. (1989), *Mathematical Methods in Classical Mechanics, 2nd Ed.*, Springer Verlag., New York.
- Asada, H. and Slotline, J.-J. E. (1986), *Robot Analysis and Control*, John Wiley & Sons, Inc., New York.
- Bühler, M. and Koditschek, D. E. (1991), 'Analysis of a simplified hopping robot.', *International Journal of Robotics Research* **10**(6), 587–605.
- Craig, J. J. (1988), *Adaptive Control of Mechanical Manipulators*, Addison-Wesley., New York.
- Craig, J. J. (1989), *Introduction to Robotics: Mechanics and Control, 2nd Ed.*, Addison-Wesley., New York.
- D'Humieres, D., Beasley, M. R., Huberman, B. A. and Lichaber, A. (1982), 'Chaotic states and routes to chaos in a forced pendulum.', *Physics Review Letters* **65**(4), 3211–3214.
- Dowell, E. H. and Pezeshki, C. (1986), 'On the understanding of chaos in Duffing's equation including a comparison with experiment.', *ASME Journal of Applied Mechanics*. **53**(3), 5–9.

- Gordon, M. K. and Shampine, L. F. (1975), *Computer Solutions of Ordinary Differential Equations: The Initial Value Problem*, W. H. Freeman & Co., San Francisco.
- Guckenheimer, J. and Holmes, P. (1983), *Nonlinear Oscillations, Dynamical Systems, and Bifurcations of Vector Fields*, Springer-Verlag., New York.
- Hübinger, B., Doerner, R., Heng, H. and Martienssen, W. (1994a), ‘Approaching nonlinear dynamics by studying the motion of a pendulum. i. observing trajectories in phase space’, *International Journal of Bifurcation and Chaos*. **4**(4), 751–760.
- Hübinger, B., Doerner, R., Heng, H. and Martienssen, W. (1994b), ‘Approaching nonlinear dynamics by studying the motion of a pendulum. ii. analyzing chaotic motions’, *International Journal of Bifurcation and Chaos*. **4**(4), 761–771.
- Hübinger, B., Doerner, R., Heng, H. and Martienssen, W. (1994c), ‘Approaching nonlinear dynamics by studying the motion of a pendulum. iii. predictability and control of chaotic motion’, *International Journal of Bifurcation and Chaos*. **4**(4), 773–784.
- Kawakami, H. (1984), ‘Bifurcations of periodic responses in forced dynamic nonlinear circuits: Computation of bifurcation values of the system parameters’, *IEEE Trans. on Circuits and Systems* **31**(4), 248–260.
- Khosla, P. K. (1986), Real-Time Control and Identification of Direct-Drive Manipulators, PhD thesis, Department of Electrical and Computer Engg, Carnegie Mellon University, USA.
- Mahout, V. (1994), Recurrences and Complex Behaviours within Robotics in the context of Repetitive Tasks - Application to a SCARA Manipulator, PhD thesis, INSA de Toulouse, no 267.
- Mahout, V., Lopez, P., Carcassés, J. P. and Mira, C. (1993), Complex behaviours of a two-revolute joints robot: harmonic, subharmonic, higher harmonic, fractional harmonic, chaotic responses., *in* ‘International Conference on Systems, Man and Cybernetics’, pp. 201–205, Vol. 5.
- M’Closkey, R. T. and Burdick, J. W. (1993), ‘Periodic motions of a hopping robot with vertical and forward motion.’, *International Journal of Robotics Research* **12**(6), 197–218.
- Moon, F. C. (1987), *Chaotic Vibrations: an Introduction for Applied Scientists and Engineers*, John Wiley & Sons, Inc., New York.
- Parker, T. S. and Chua, L. O. (1989), *Practical Numerical Algorithms for Chaotic Systems*, Springer Verlag., New York.

- Paul, R. P. (1981), *Robot Manipulators: Mathematics, Programming and Control*, MIT press, Cambridge, Mass.
- Sekar, P. and Narayanan, S. (1992), 'Chaos in mechanical systems - a review', *Sadhana*. **20**(3), 341–748.
- Shrinivas, L. and Ghosal, A. (1996), Possible chaotic motions in a feedback controlled 2R robot., in 'Proceedings of IEEE Conference on Robotics and Automation, Minneapolis', pp. 1241–1246.
- Spong, M. W. (1992), Remark on robot dynamics : Canonical transformations and Riemannian geometry, in 'International Conference on Robotics and Automation', pp. 554–559.
- Stoker, J. J. (1969), *Differential Geometry*, John Wiley & Sons, Inc., New York.
- Streit, D. A., Krousgrill, C. M. and Bajaj, A. K. (1986), 'A preliminary investigation of the dynamic stability of flexible manipulators performing repetitive tasks.', *Trans. of the ASME : Journal of Dynamic Systems, Measurement and Control* **108**(6), 206–214.
- Tongue, B. H. (1986), 'On necessary and sufficient conditions for chaos in Duffing's equation : An heuristic approach.', *Journal of Sound and Vibration*. **110**(1), 59–78.
- Vakakis, A. F. and Burdick, J. W. (1990), Chaotic motions in the dynamics of a hopping robot., in 'Proceedings of IEEE International Conference on Robotics and Automation.', pp. 1464–1469.
- Vakakis, A. F. and Burdick, J. W. (1991), 'An "interesting" strange attractor in the dynamics of a hopping robot.', *International Journal of Robotics Research* **10**(6), 606–618.
- Varghese, M., Fuchs, A. and Mukundan, R. (1991), 'Chaotic zero dynamics in kinematically redundant robots.', *IEEE Trans. on Aerospace and Electronic Systems* **27**(5), 784–796.
- Wolf, A., Swift, J. B., Swinney, H. A. and Vastano, J. A. (1985), 'Determining Lyapunov exponents from a time series.', *Physica 16D* **16D**, 285–317.
- Zak, M. (1985a), 'Criteria for chaos in non-linear mechanics', *Int. J. Nonlinear Mechanics*. **21**(3), 175–182.
- Zak, M. (1985b), 'Two types of chaos in non-linear mechanics', *Int. J. Nonlinear Mechanics*. **20**(4), 297–308.

Captions of figures

- Figure 1: Surface with Gaussian curvature less and greater than zero.
- Figure 2: The PP robot
- Figure 3: The PR robot
- Figure 4: The RP robot
- Figure 5: The RR robot
- Figure 6: The RRR robot
- Figure 7: The RRP robot
- Figure 8: Phase plot for non chaotic parameters for RP robot with PD control.
- Figure 9: Phase plot for chaotic parameters for RP robot with PD control.
- Figure 10: Lyapunov exponent for chaotic parameters for RP robot with PD control.
- Figure 11: Lyapunov exponent for non chaotic parameters for RP robot with PD control.
- Figure 12: Poincaré map for chaotic parameters.
- Figure 13: Chaos map for PD control of RP robot.
- Figure 14: Chaos map for model-based control of RP robot.
- Figure 15: Bifurcation diagram for θ_1 for RP robot with PD control.
- Figure 16: Bifurcation diagram for X for RP robot with PD control.
- Figure 17: Largest Lyapunov exponent for RR robot with PD and model based control.
- Figure 18: Chaos map for RR robot under PD control.
- Figure 19: Chaos map for RR robot under model based control($\epsilon = -0.9$).
- Figure 20: Bifurcation diagram for RR robot under model based control.

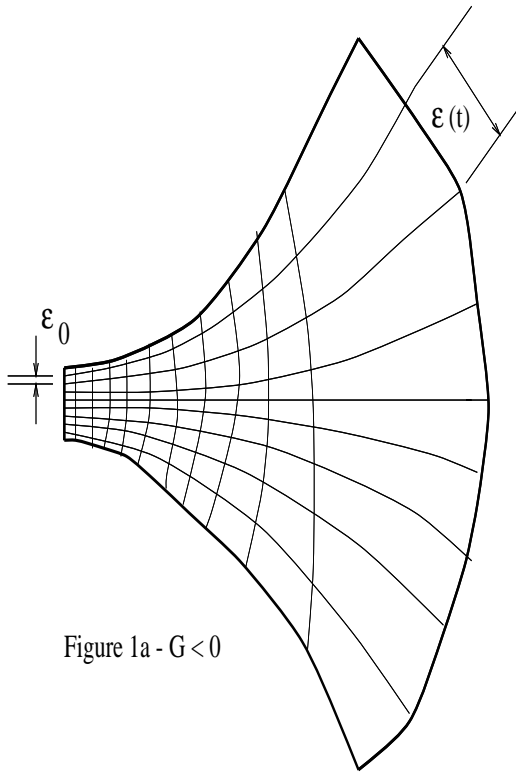


Figure 1a - $G < 0$

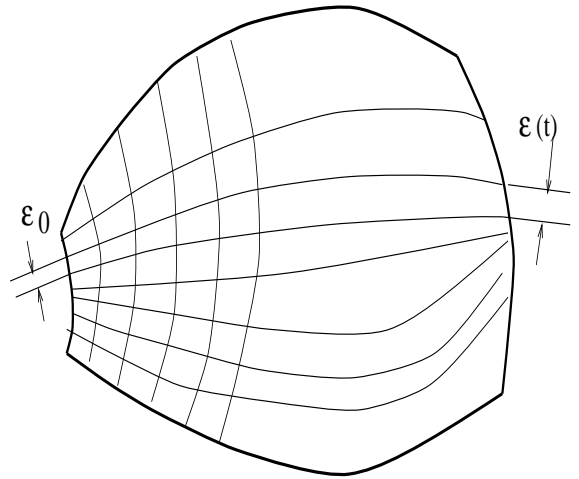


Figure 1b - $G > 0$

Figure 1: Surface with Gaussian curvature less and greater than zero

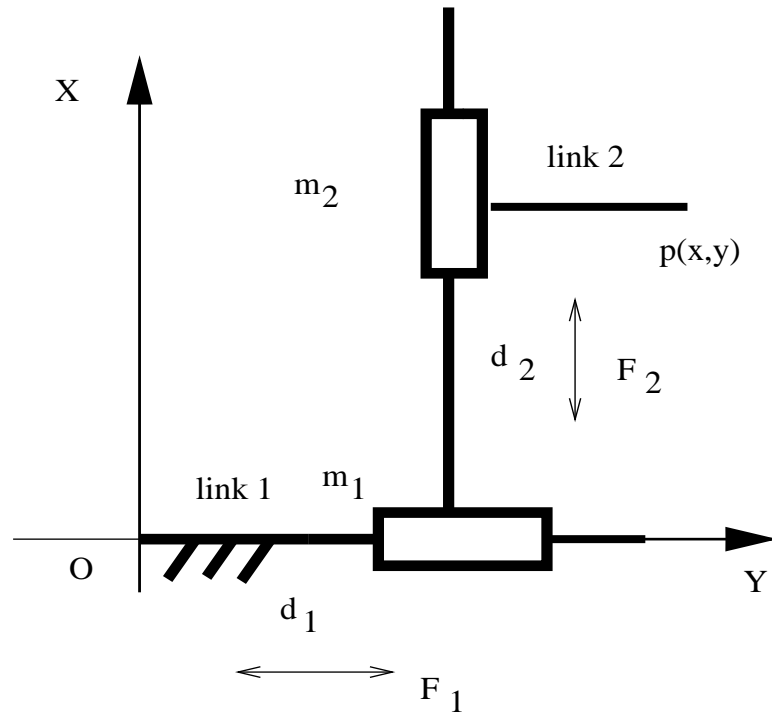


Figure 2: The PP robot

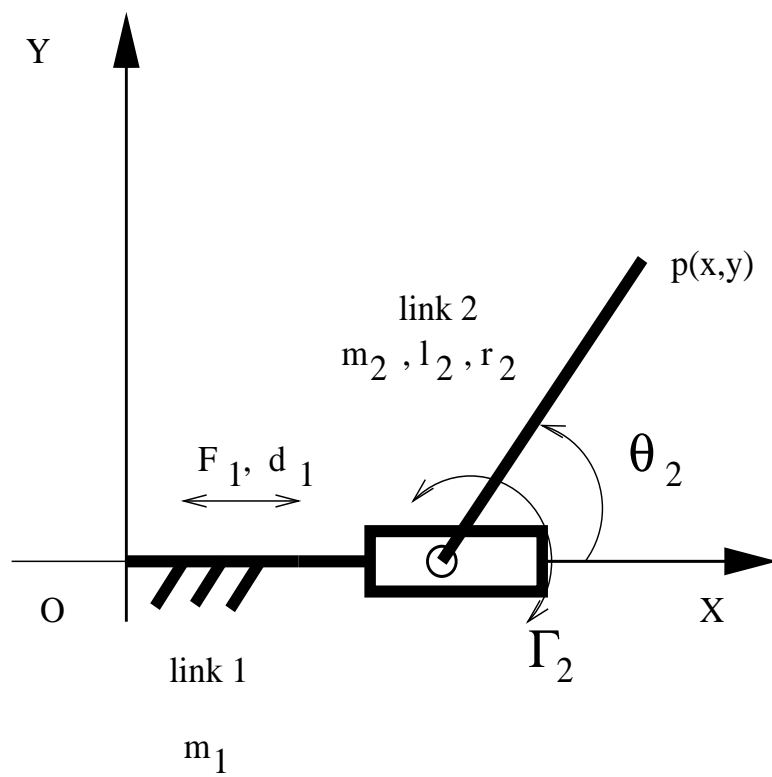


Figure 3: The PR robot

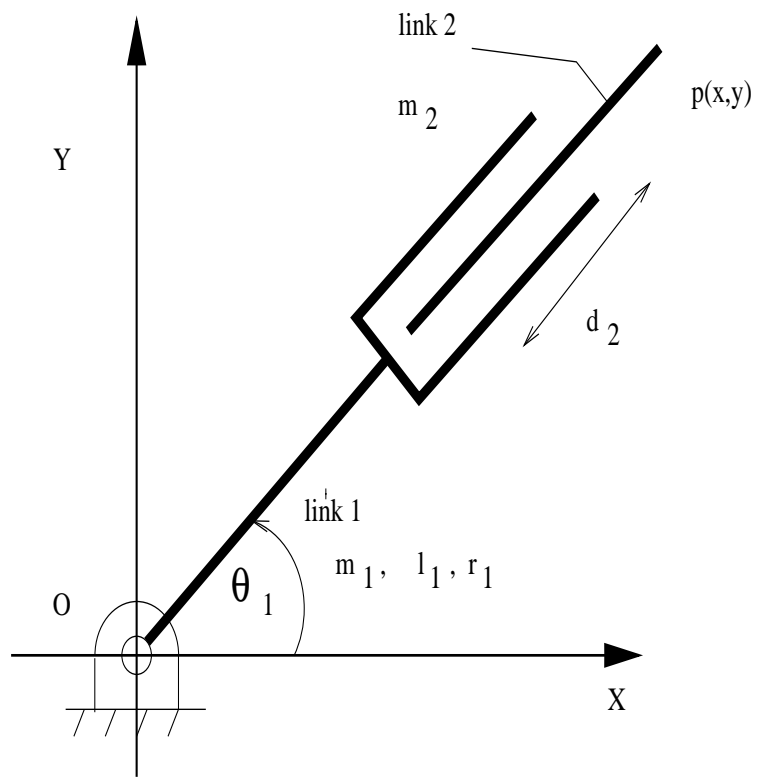


Figure 4: The RP robot

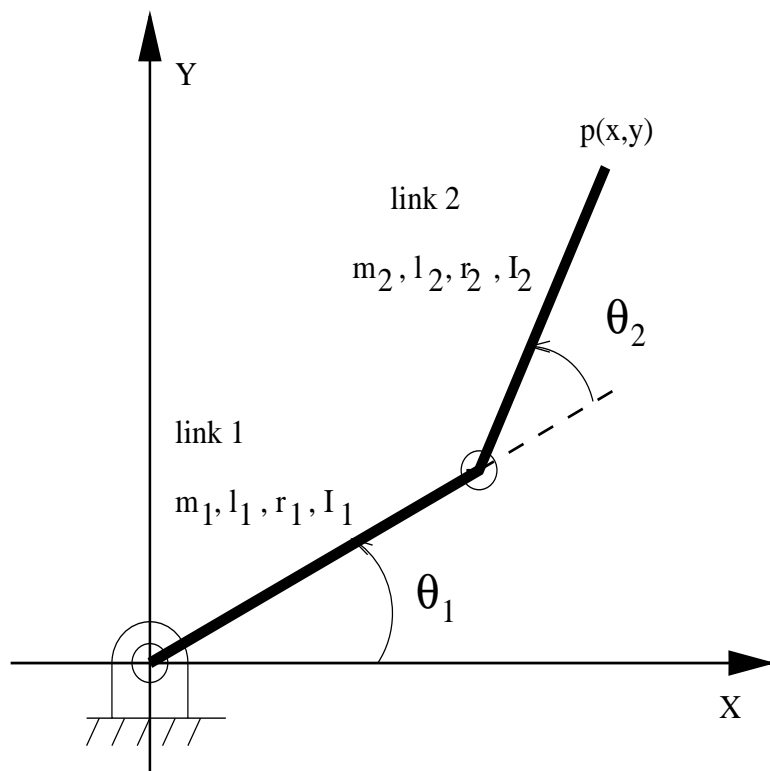


Figure 5: The RR robot

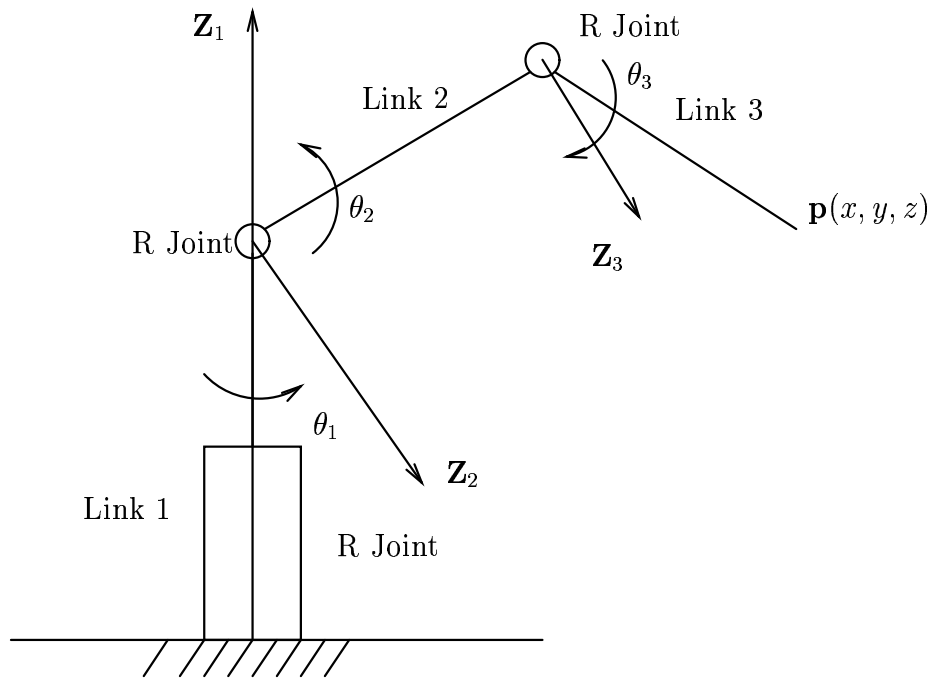


Figure 6: The RRR robot

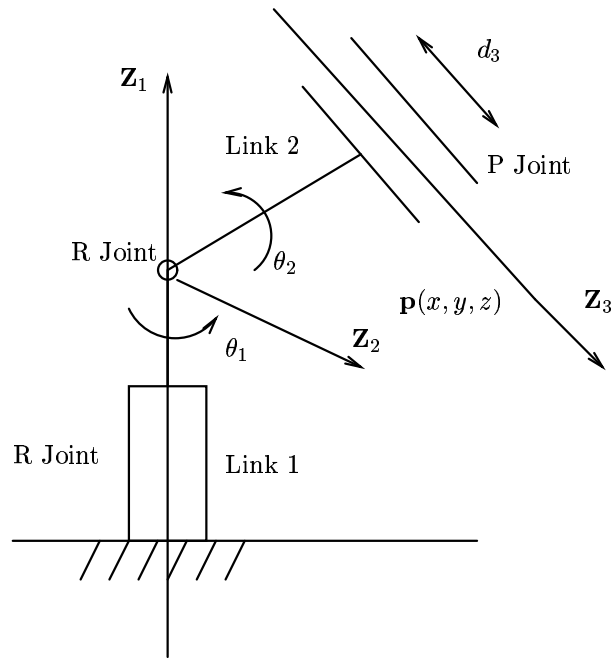


Figure 7: The RRP robot

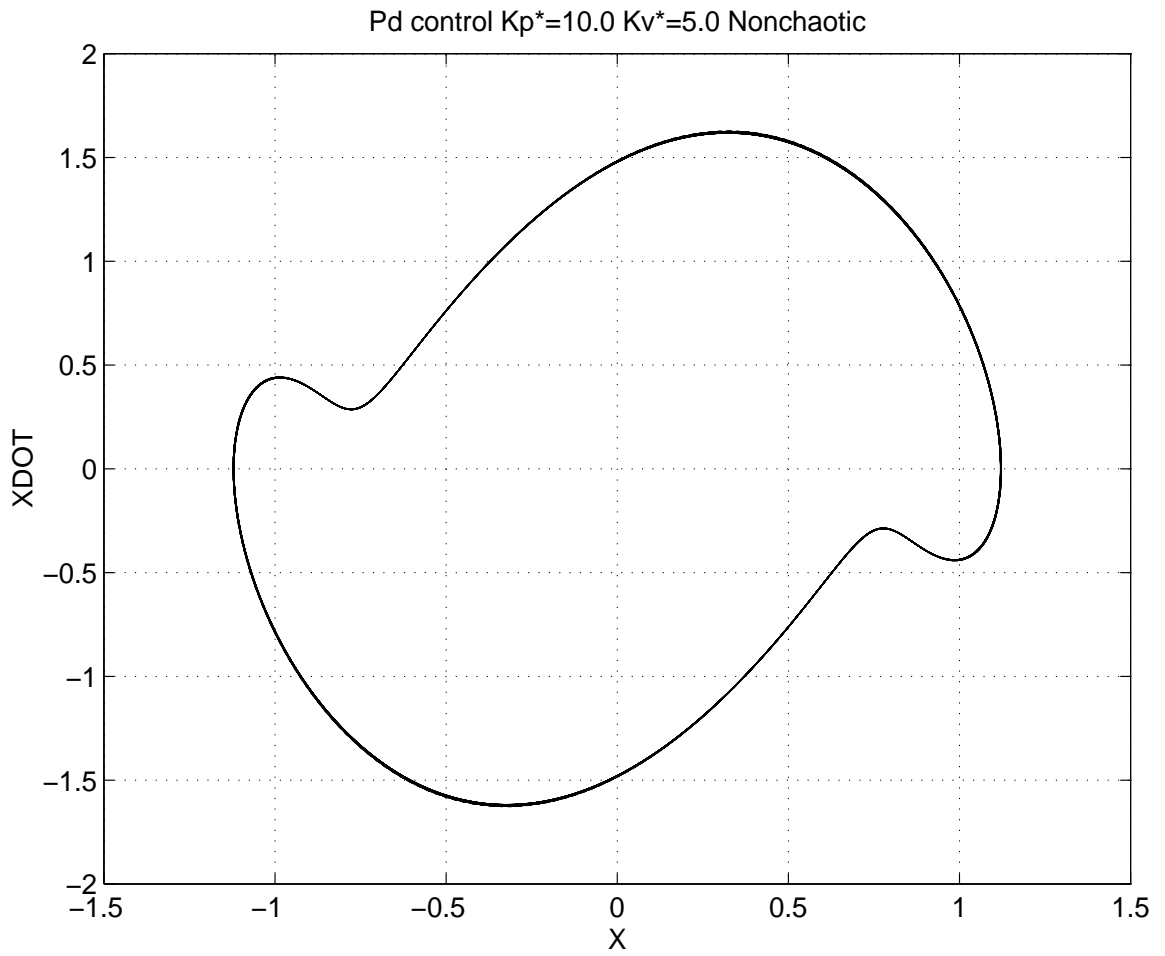


Figure 8: Phase plot for non chaotic parameters for RP robot with PD control.

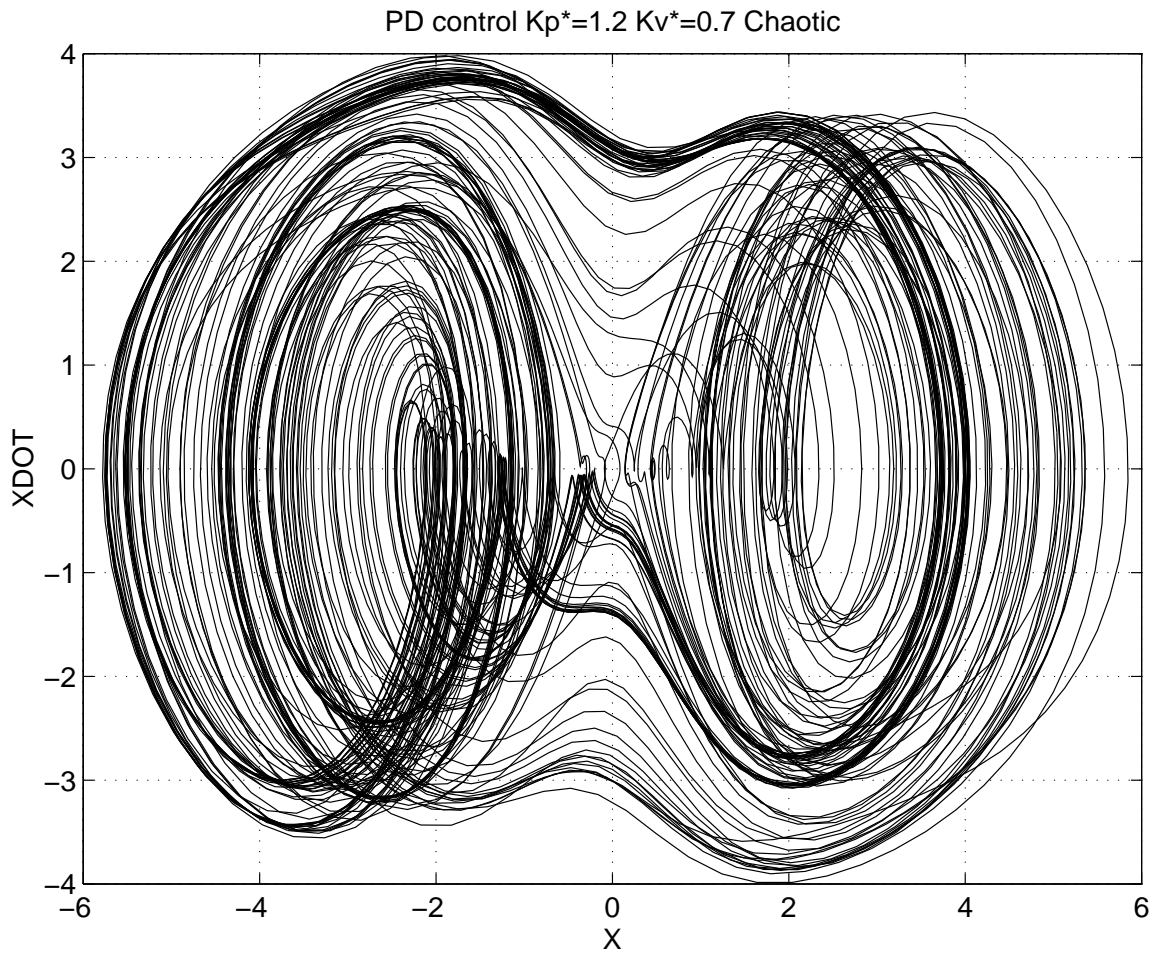


Figure 9: Phase plot for chaotic parameters for RP robot with PD control.

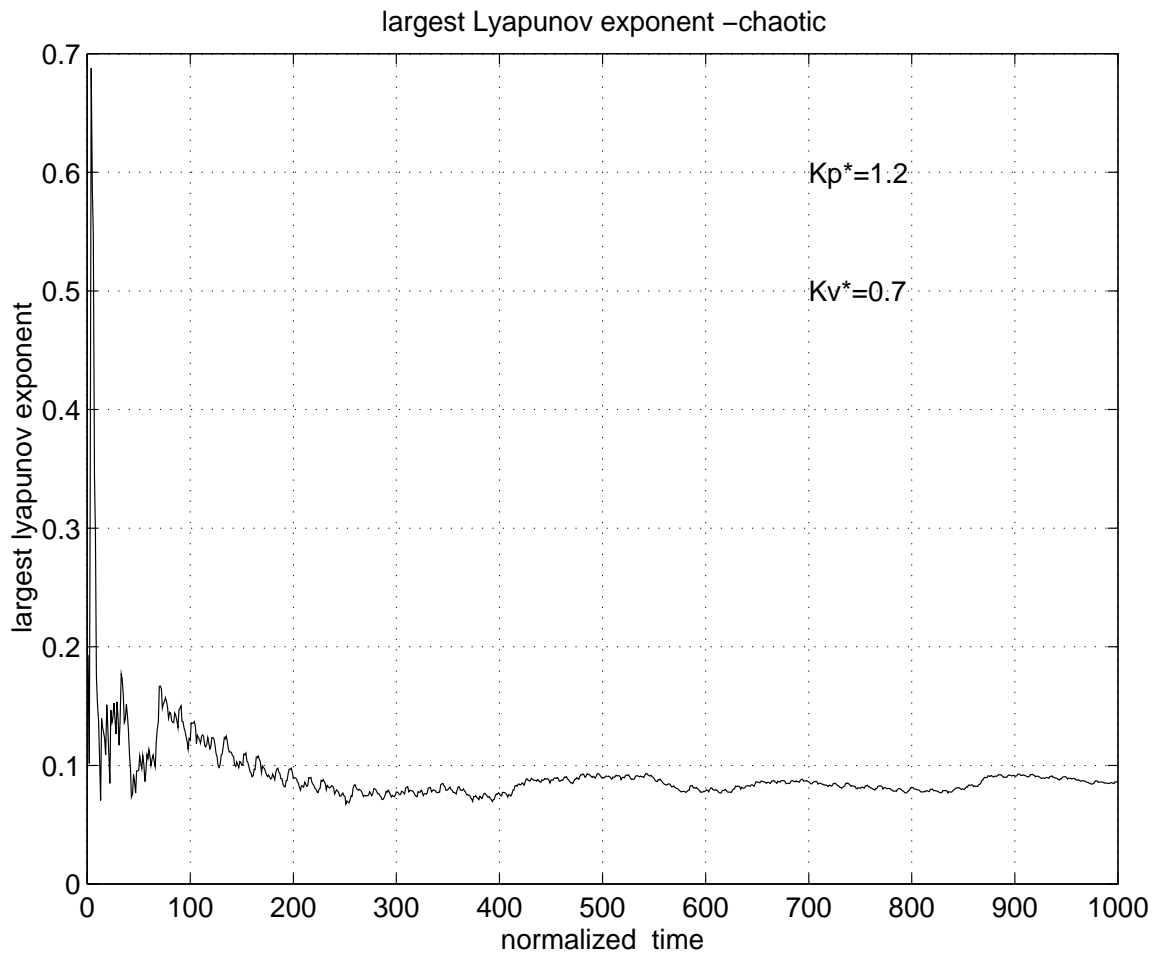


Figure 10: Lyapunov exponent for chaotic parameters for RP robot with PD control

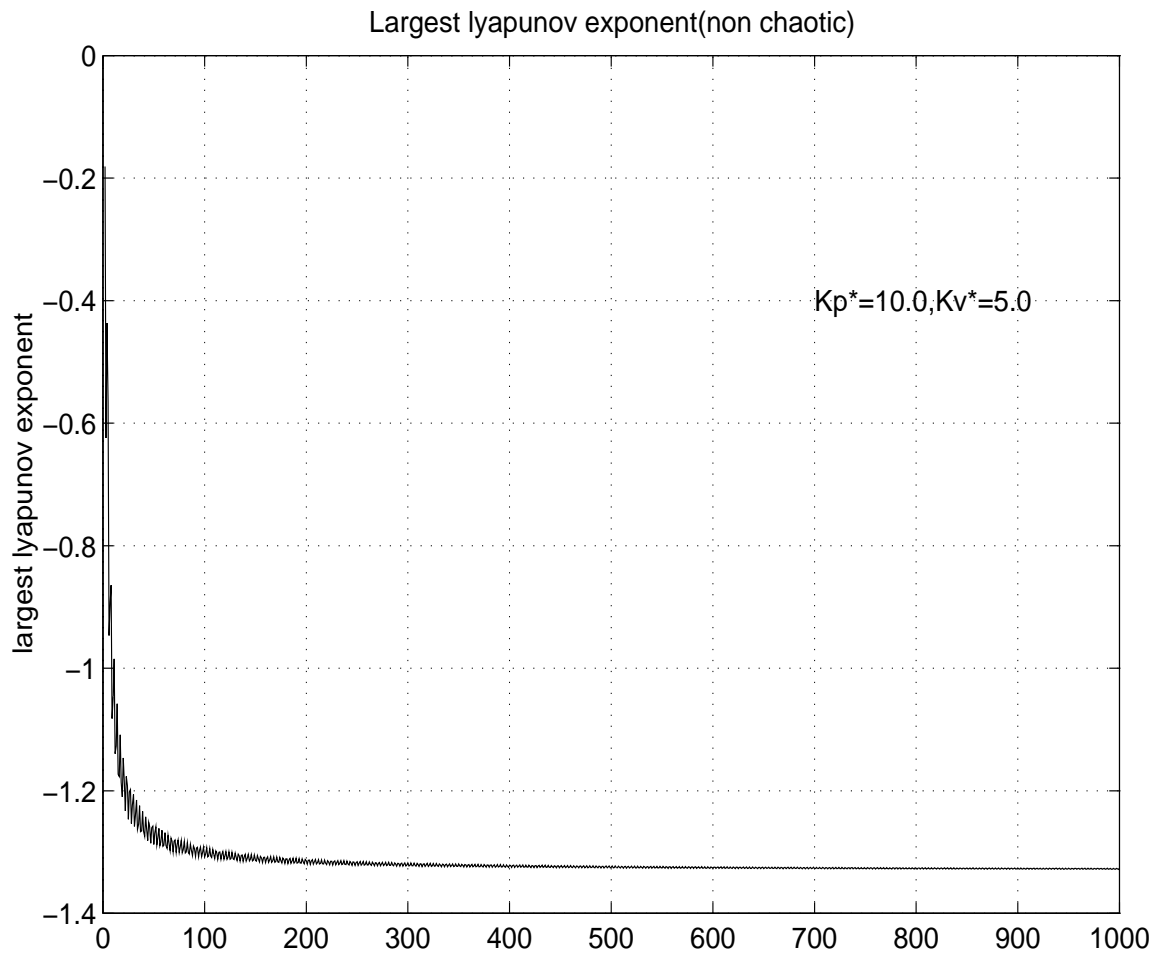


Figure 11: Lyapunov exponent for non chaotic parameters for RP robot with PD control

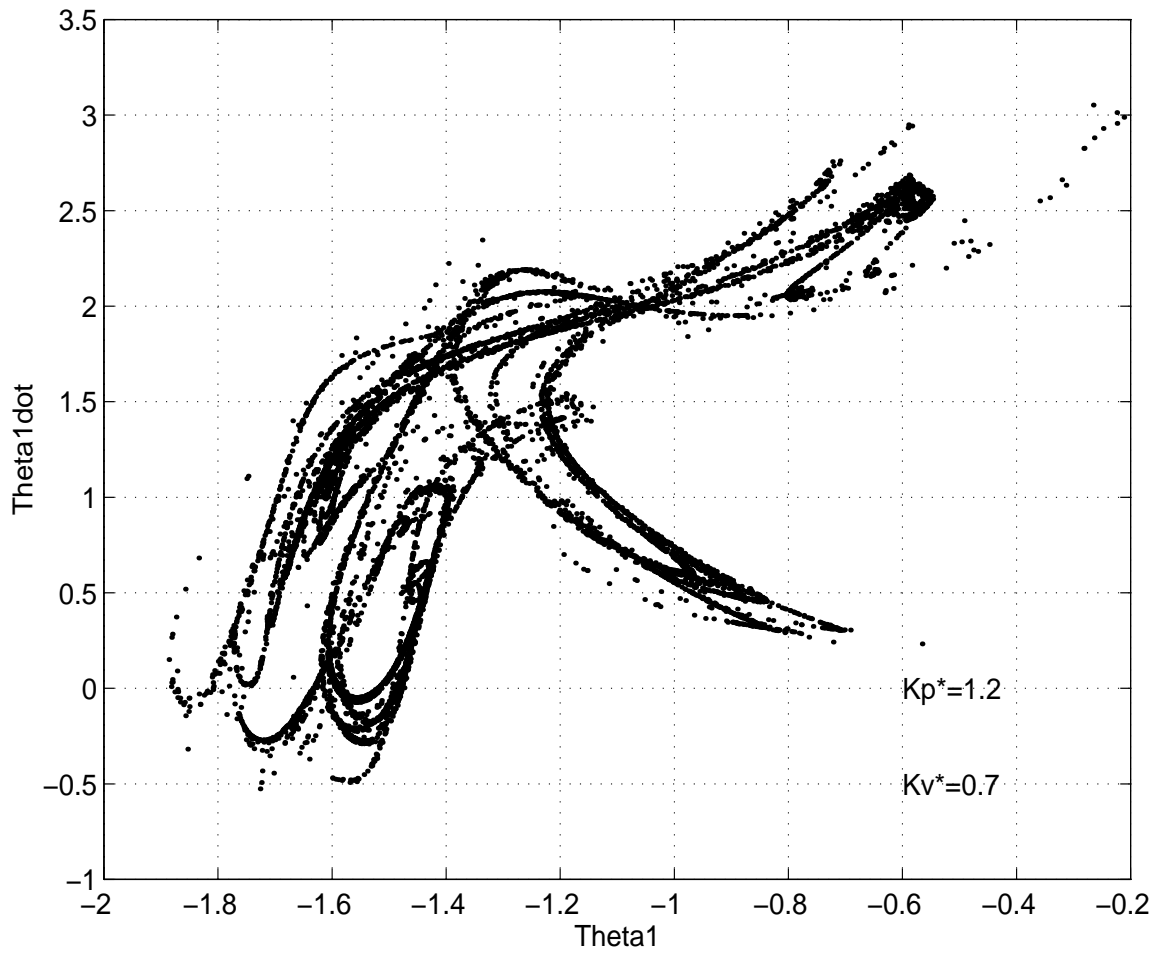


Figure 12: Poincaré map for chaotic parameters

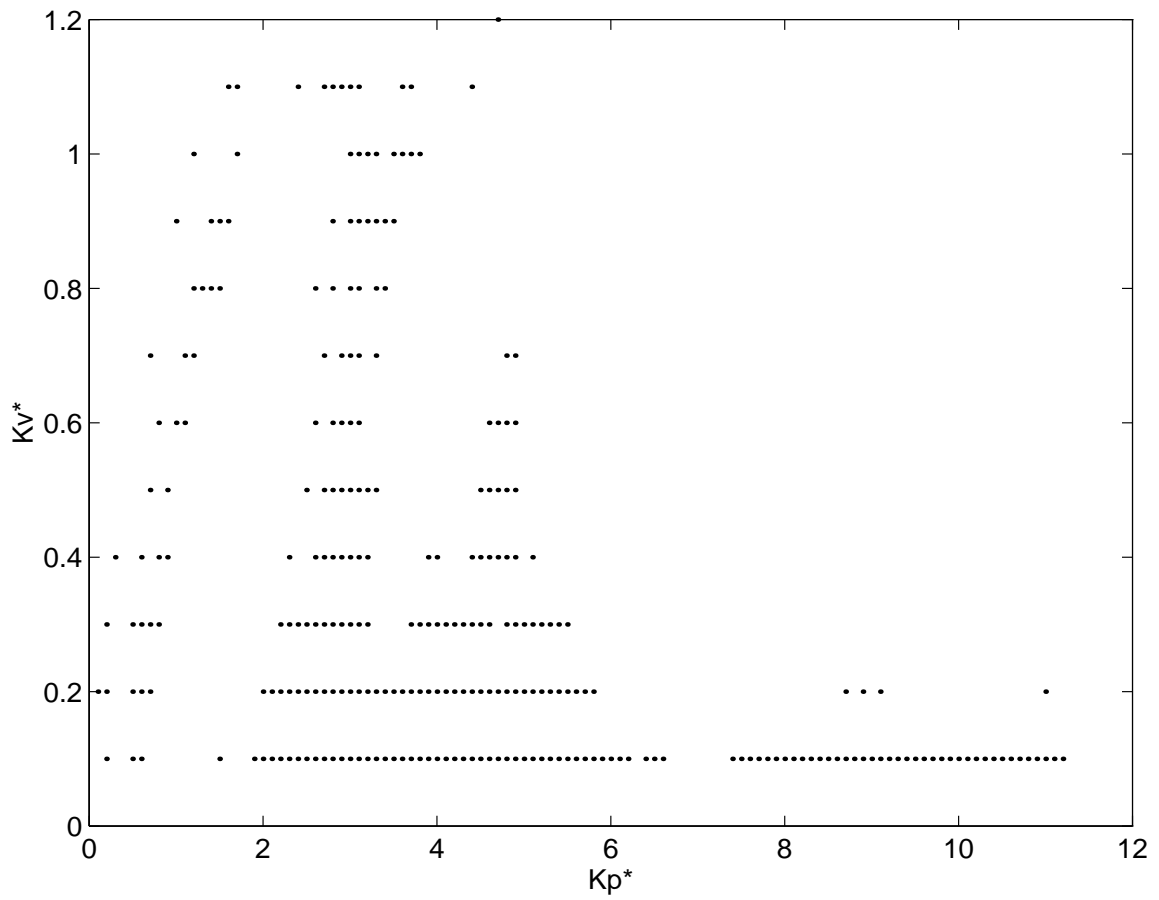


Figure 13: Chaos map for PD control of RP robot

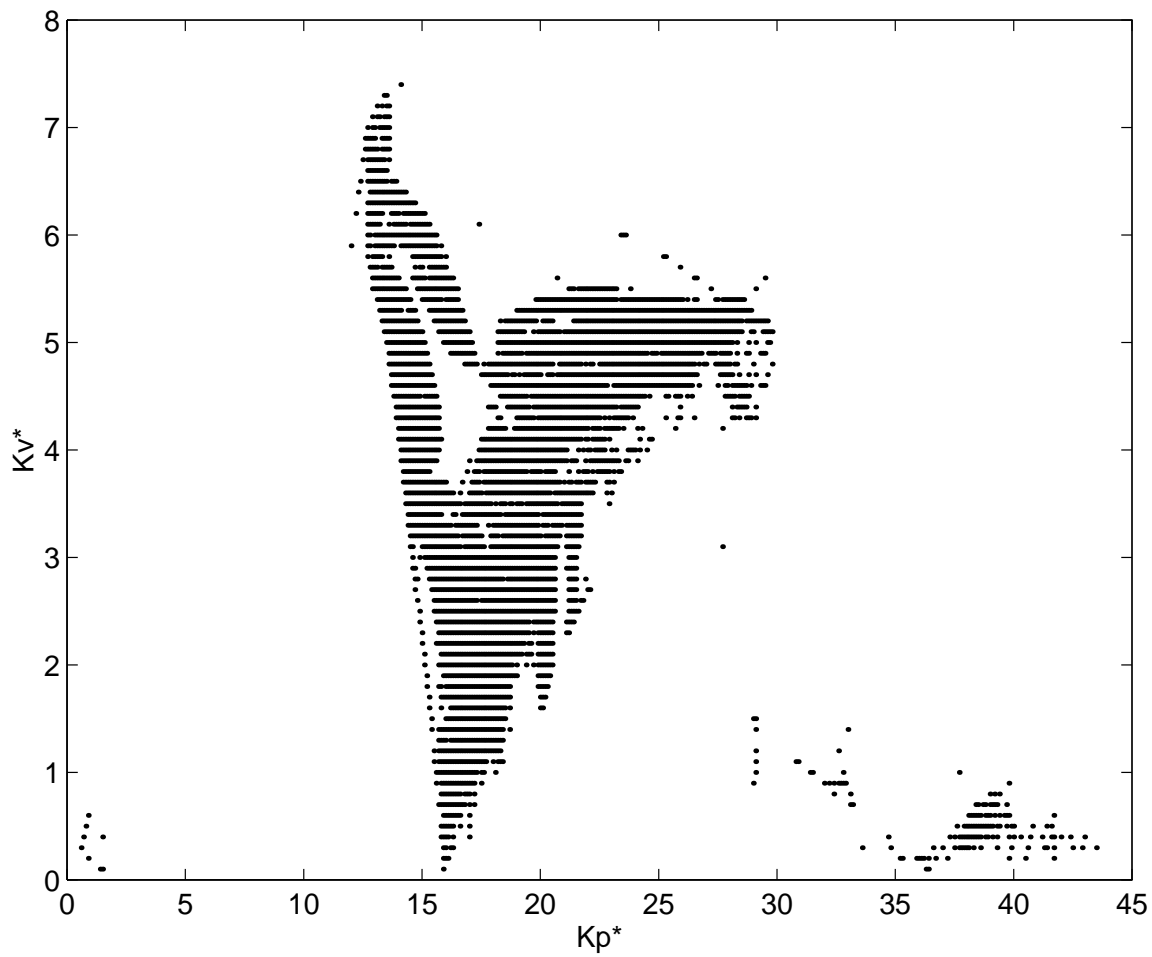


Figure 14: Chaos map for model-based control of RP robot

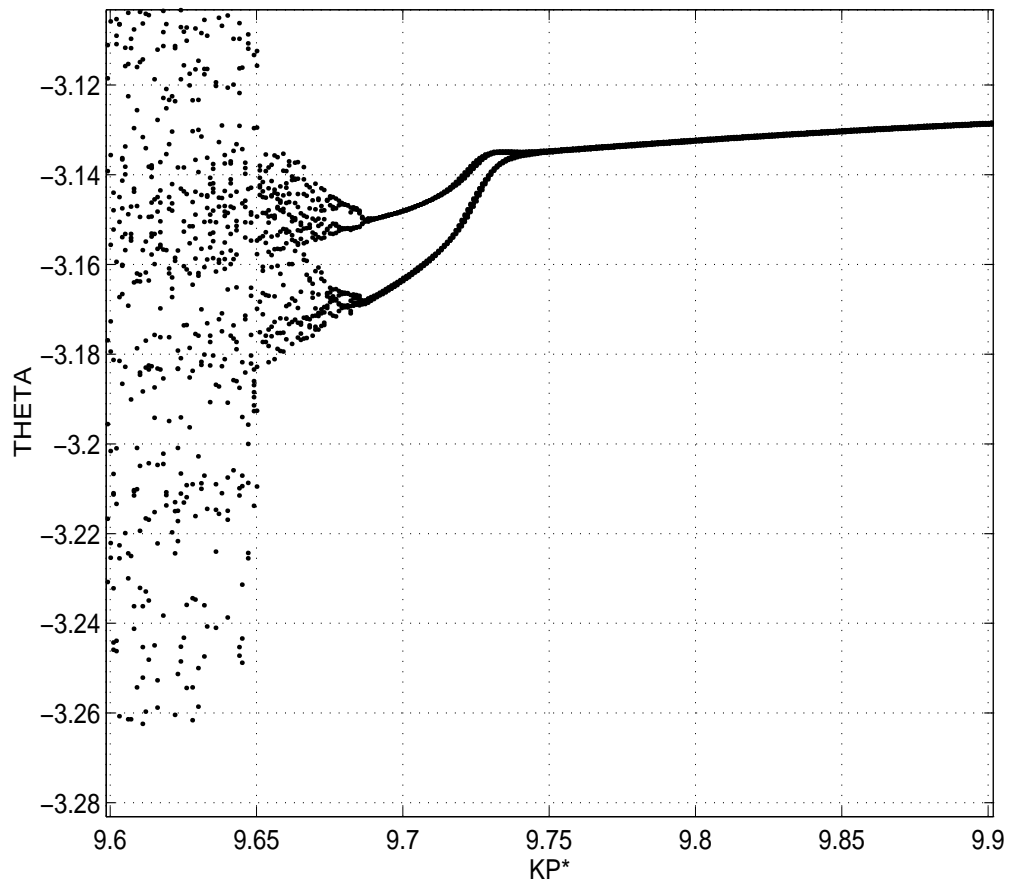


Figure 15: Bifurcation diagram for θ_1 for RP robot with PD control

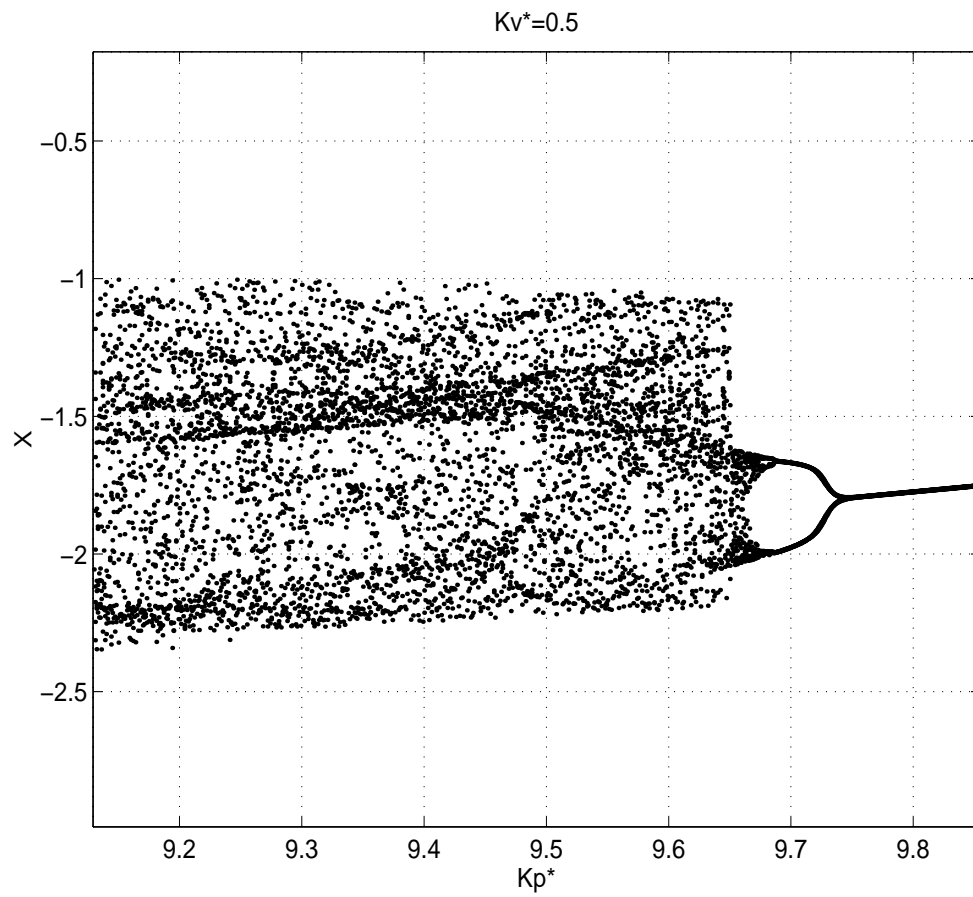


Figure 16: Bifurcation diagram for X for RP robot with PD control

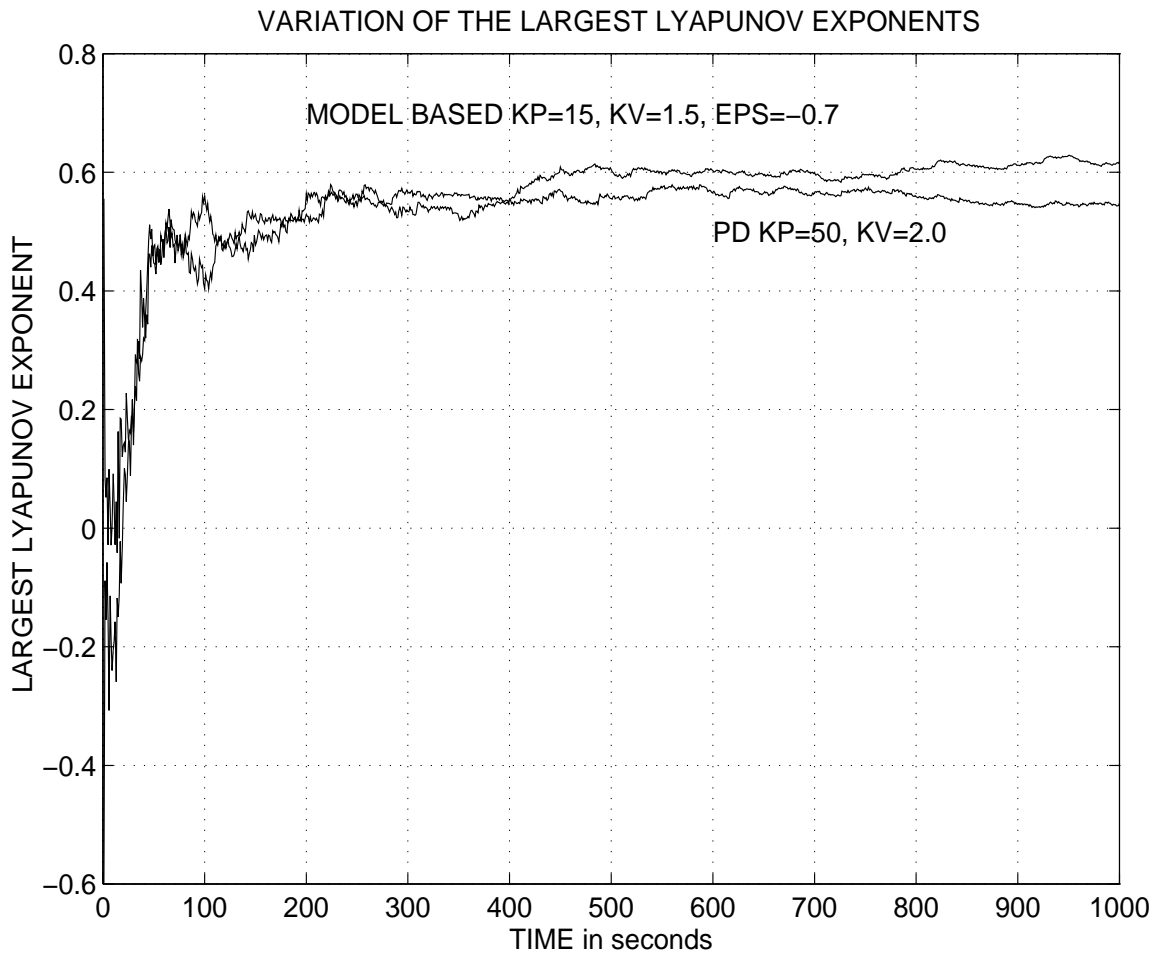


Figure 17: Largest Lyapunov exponent for RR robot with PD and model based control

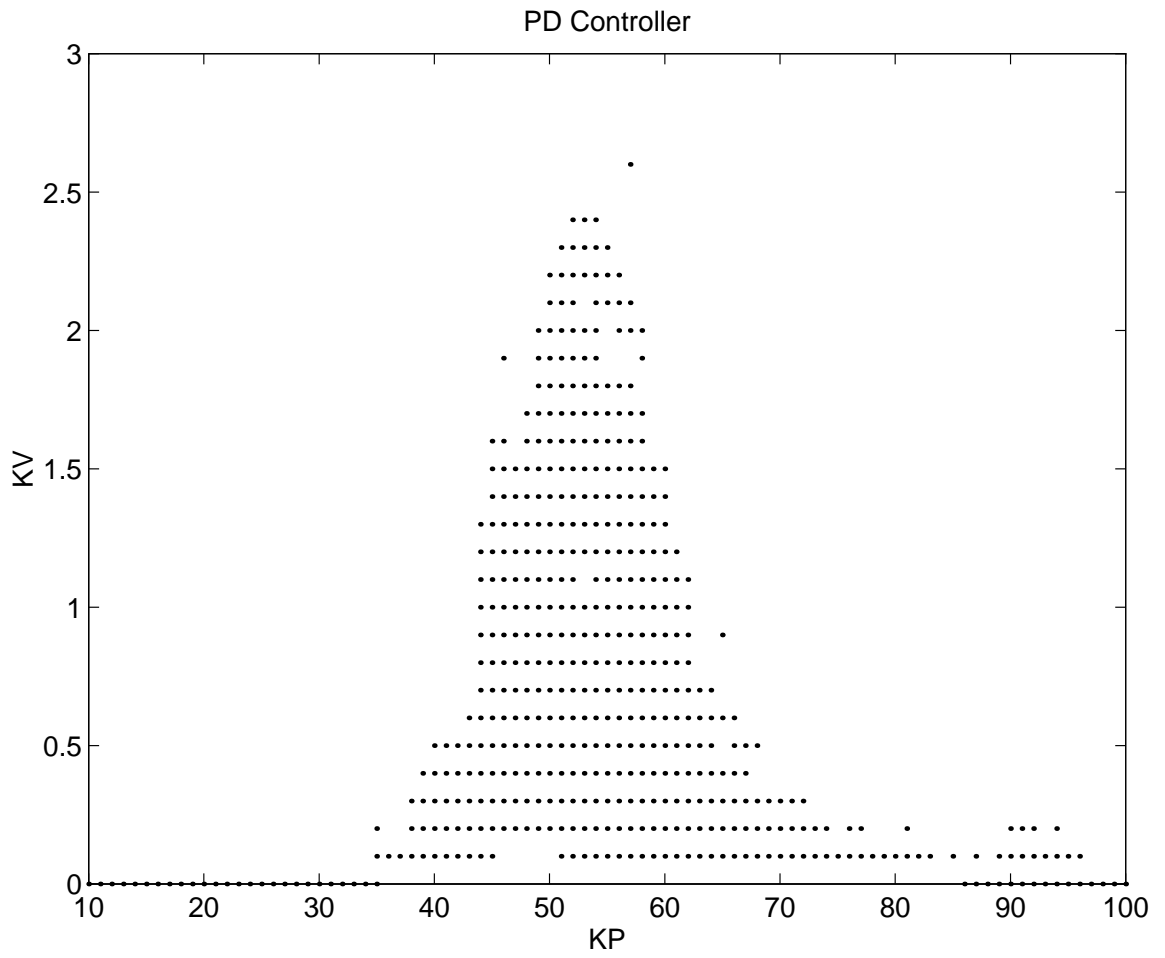


Figure 18: Chaos map for RR robot under PD control

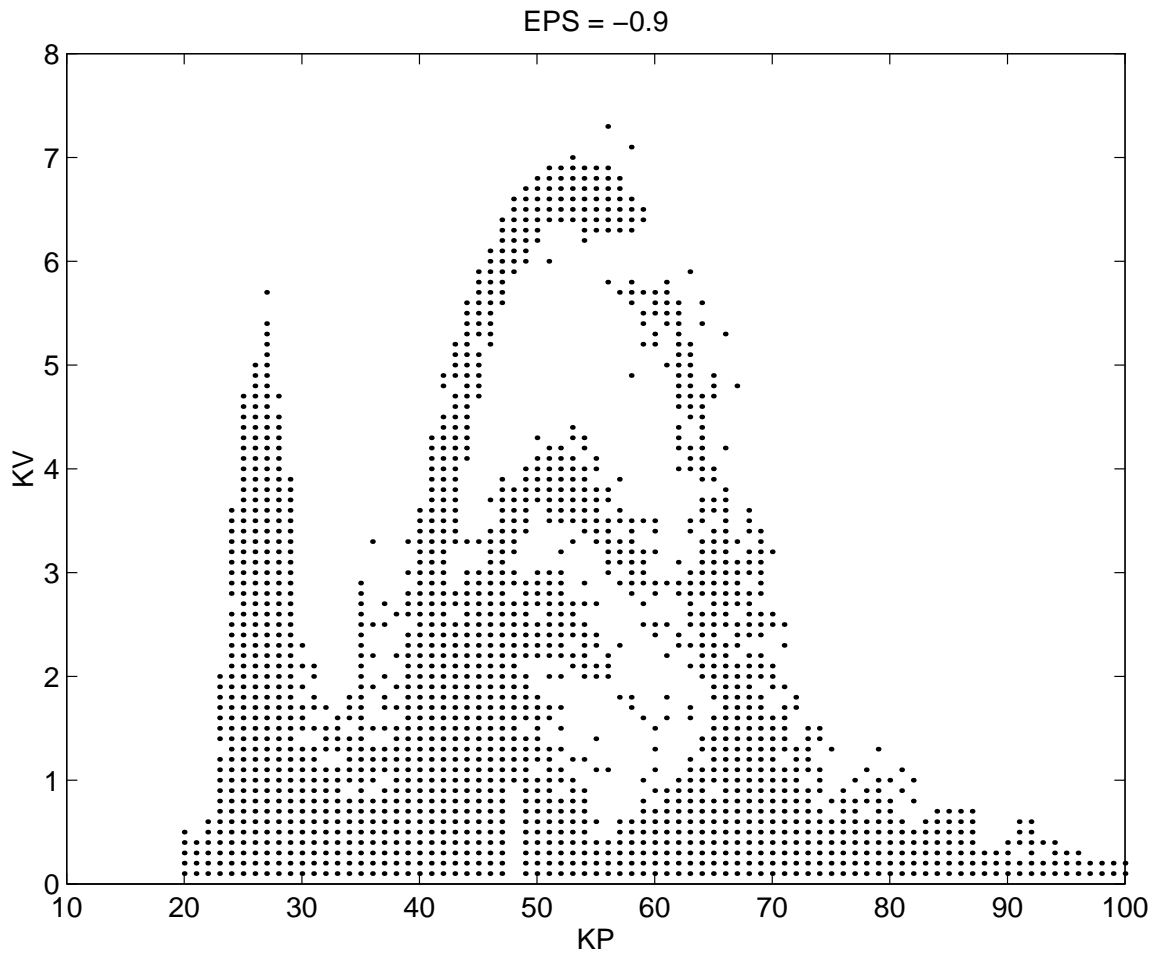


Figure 19: Chaos map for RR robot under model based control($\epsilon = -0.9$)

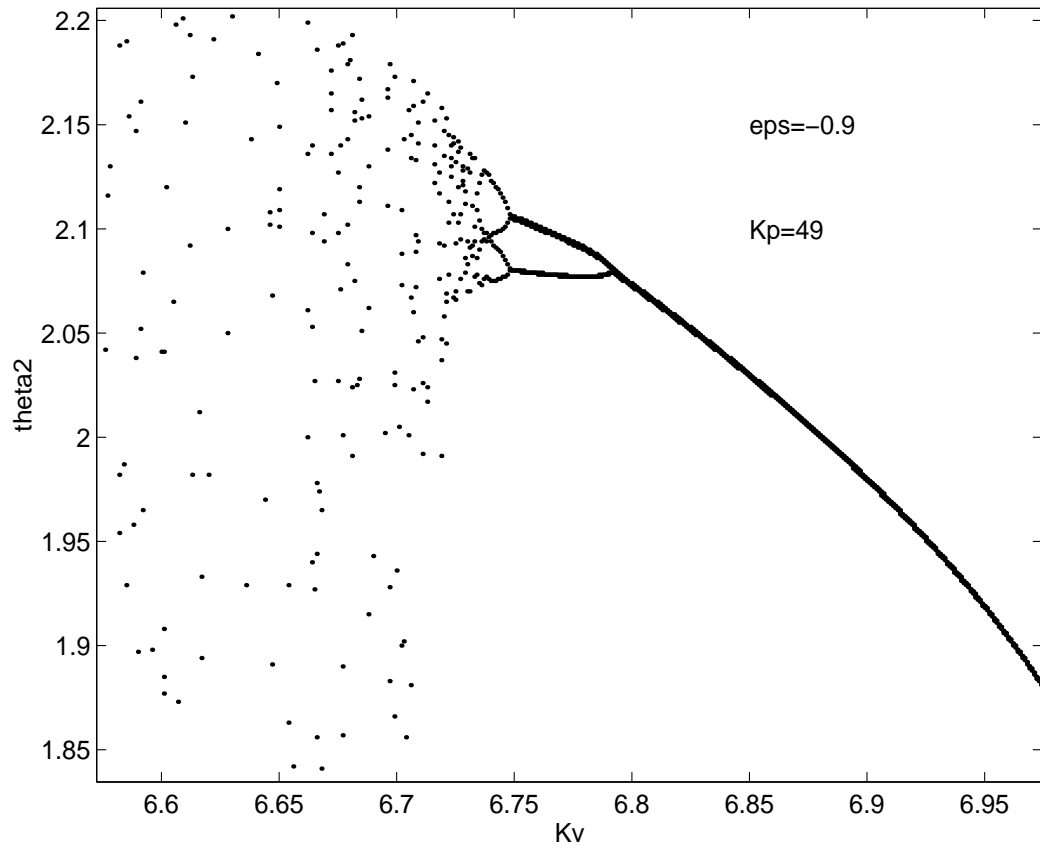


Figure 20: Bifurcation diagram for RR robot under model based control